lubricants

Review

Effect of Humidity on Friction and Wear—A Critical Review

Zhe Chen [1], Xin He [1], Chen Xiao [2] and Seong H. Kim [1,2,*]

[1] Department of Chemical Engineering and Materials Research Institute, Pennsylvania State University, University Park, PA 16802, USA; zuc191@psu.edu (Z.C.), xuh118@psu.edu (X.H.)
[2] Tribology Research Institute, State Key Laboratory of Traction Power, Southwest Jiaotong University, Chengdu 610031, China; chenxiao@my.swjtu.edu.cn
* Correspondence: shkim@engr.psu.edu; Tel.: +1-814-863-4809

Received: 22 July 2018; Accepted: 20 August 2018; Published: 22 August 2018

Abstract: The friction and wear behavior of materials are not intrinsic properties, but extrinsic properties; in other words, they can drastically vary depending on test and environmental conditions. In ambient air, humidity is one such extrinsic parameter. This paper reviews the effects of humidity on macro- and nano-scale friction and wear of various types of materials. The materials included in this review are graphite and graphene, diamond-like carbon (DLC) films, ultrananocrystalline diamond (UNCD), transition metal dichalcogenides (TMDs), hexagonal boron nitride (h-BN), boric acid, silicon, silicon oxide, silicates, advanced ceramics, and metals. Details of underlying mechanisms governing friction and wear behaviors vary depending on materials and humidity; nonetheless, a comparison of various material cases revealed an overarching trend. Tribochemical reactions between the tribo-materials and the adsorbed water molecules play significant roles; such reactions can occur at defect sites in the case of two-dimensionally layered materials and carbon-based materials, or even on low energy surfaces in the case of metals and oxide materials. It is extremely important to consider the effects of adsorbed water layer thickness and structure for a full understanding of tribological properties of materials in ambient air.

Keywords: humidity; friction; wear

1. Introduction

Friction and wear are ubiquitous in daily life. Under most circumstances, friction and wear come with energy consumption and material loss. In order to reduce friction and wear and thus save energy and resources, it is vital to understand the tribological properties of materials involved in such processes in ambient conditions.

It is well known that tribological properties are not just intrinsic or inherent properties of materials, but are strongly dependent on working conditions. The working condition includes not only operating parameters (contact pressure, sliding speed, and counterpart materials), but also environmental factors (temperature, humidity, and atmosphere, among others). In ambient air, the impacts of environmental factors pertain to unlubricated or solid-lubricated conditions. Among all the factors mentioned above, humidity could be the easiest one to be ignored, because the adsorption of water is invisible and it is commonly believed that reactions between water and tribo-materials are normally self-limited only to the topmost surface at ambient temperatures. Or sometime, the physisorbed water molecules at the sliding interface are considered as a lubricant. Although reasonable based on common sense, it could be wrong if interfacial stress is involved. During the process of rubbing or sliding, water can react with the tribo-material due to normal load and shear stress, and further influence friction and wear behavior.

Lubricants **2018**, *6*, 74; doi:10.3390/lubricants6030074

This paper aims at reviewing the humidity dependence of the friction and wear behaviors of materials commonly used as solid lubricants or tribo-elements and the underlying mechanisms. Relative humidity (RH), which is defined as the ratio of the partial pressure of water vapor to the equilibrium vapor pressure of water at a given temperature, is commonly used to quantify environmental humidity. The materials concerned here include graphite and graphene, diamond-like carbon (DLC) films, ultra-nanocrystalline diamond (UNCD), transition metal dichalcogenides (TMDs), hexagonal boron nitride (h-BN), boric acid, silicon, silicon oxide, silicates, advanced ceramics and metals. Beside the conventional tribo-tests at the macroscale, nanoscale tribological tests based on atomic force microscopy (AFM) are also involved. It was wished for but not possible to cover all published data on humidity dependence in the literature; in this review paper, overarching trends rather than individual cases are discussed. Moreover, it should be noted that although some contradictory results were reported in the literature, only recent experimental results with reasonable explanations are selected in this review. Some older data can be found in another review paper and references therein [1].

2. Graphite and Graphene

The study of humidity effects on the friction and wear properties of graphite dates back to the 1930s, when graphite was used as a solid lubricant for electric brushes [2–4]. Systematic researches on the effect of humidity was conducted after it was found that the graphite electric brushes suffered from severe wear in airplanes flying at high altitudes, where the humidity is low [4]. It was found that both the friction and wear of graphite decrease as the water vapor pressure or humidity increases [4–11]. Based on these experimental observations, it was realized that the good lubricity of graphite is not an intrinsic property, but one influenced by environmental factors.

In the early stage, two mechanisms were put forward to explain the humidity dependence. In the first mechanism, which was suggested by Savage, the surfaces of graphite are covered by a monolayer of condensable water molecules, which present a surface of low cohesive energy that is analogous to a boundary oil film covering a metal [5,7]. The second mechanism, which was proposed by Rowe and Bryant, found that water molecules can be chemisorbed in graphite by reaction with π electrons, thus forming some intercalation products and weakening the interlayer bond, making interlayer sliding easier [9,10]. Later, Rowe and Bryant's hypothesis was disputed. It was found that the thickness of the graphite crystal and the interlayer distance near the graphite surface do not change under various environmental humidity conditions [12,13].

Then, the fact that the edge sites on graphite surface are much more reactive than the basal planes was linked to the friction and wear properties of graphite. Lancaster found that graphite exhibits large and sudden increases in friction and wear at a critical contact temperature, which results from frictional heat under certain combinations of load, speed and ambient temperature. He attributed the phenomenon to the insufficient water vapor available from the environment for the formation of an adsorbed film [14–16]. He also proposed that the adsorbed vapor on the basal plane of graphite functions as a 'reservoir' from which molecules can migrate to neutralize edge sites being continuously exposed during the normal, low-wear regime [17]. It was initially believed that the adsorption of water molecules onto the graphite surface was physisorption of molecular water until Lepage proposed that it is actually dissociative chemisorption of water leading to H and OH radicals [18]. This proposal was later proved through density functional theory (DFT) based simulation [19–22] and mass spectrometry analysis of the ball milling products of heavy water (D_2O) and graphite [23].

After the discovery of graphene, the friction and wear properties of graphene became a hot topic. Graphene shows great lubricity as a coating material [24–26]. Similar to graphite, when the graphene coating is rubbed with a macroscale counterpart, the friction and wear decreases as the environmental humidity increases [26–28]. As shown in Figure 1, the phenomenon was attributed to the dissociative chemisorption of water at carbon dangling bond sites exposed upon rupture of graphene. However, when the counter part is a nanoscale AFM tip rather than a conventional macroscale ball or pin and humidity increases [26–28]. As shown in Figure 1, the phenomenon was attributed to the dissociative chemisorption of water at carbon dangling bond sites exposed upon rupture of graphene. However, when the counter part is a nanoscale AFM tip rather than a conventional macroscale ball or pin and the scan size is small enough that the sliding contact occurs only at the basal plane instead of a mixture of basal planes and edges, the presence of a small amount of water does not strongly influence friction on flat terraces [29,30]. Instead, it was shown that friction at atomic steps can increase with water adsorption [29]. Systematic researches on the effect of humidity on the friction and wear properties of graphene are believed to be currently under way.

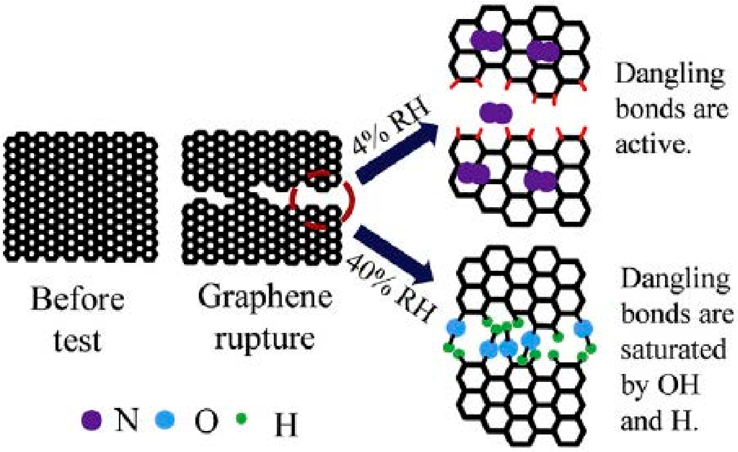

Figure 1. Schematics of the passivation of the newly generated graphene edges through water dissociative chemisorption [27].

3. Diamond-Like Carbon (DLC)

DLC is an amorphous carbon material that draws great interest for coating applications for wear prevention and solid lubrication. Depending on the hydrogen content, including both chemically bonded and interstitial hydrogen, DLC films can be classified as non-hydrogenated DLC (a-C) or hydrogenated DLC (a-C:H or H-DLC) films [31–37]. These two kinds of DLC films possess very different mechanical, electrical, optical and tribological properties. Conventionally, it was believed that DLC surfaces are hydrophobic. However, it should be noted that DLC surfaces can get oxidized readily upon exposure to air [38], and water can physisorb on the oxidized DLC surface, exhibiting typical type-II adsorption isotherm (Figure 2) [39].

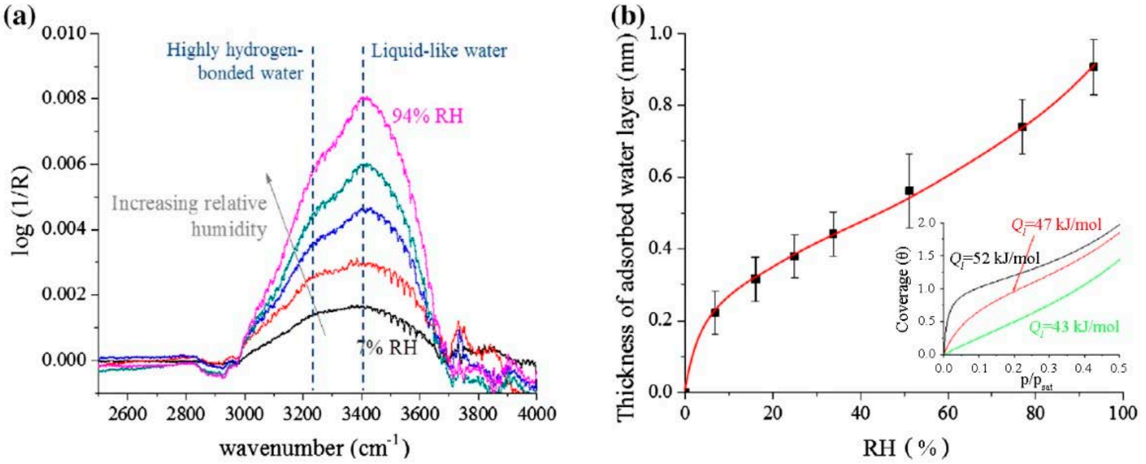

Figure 2. (**a**) ATR-IR spectra of water adsorbed on DLC surface from humid ambient. (**b**) Adsorption isotherm of water on DLC. Inset to (**b**) shows BET adsorption isotherms simulated for three cases. The heat of adsorption (Q_i) is significantly higher (52 kJ/mol) than, slightly higher (47 kJ/mol) than, and comparable (43 kJ/mol) to the heat of liquefaction of water (42.06 kJ/mol) [39].

Tribologically, a-C:H films attract much more attention than a-C films, because a superlow coefficient of friction (COF) can be achieved by a-C:H films in inert gas or vacuum environments [40–48]. There are several models to explain this superlubricity; the most highly cited mechanism assumes that the hydrogen-termination of the carbon surfaces leads to little or no chemical or physical interactions during sliding contacts [48–50]. However, the superlow COF cannot be maintained in humidity

Tribologically, a-C:H films attract much more attention than a-C films, because a superlow coefficient of friction (COF) can be achieved by a-C:H films in inert gas or vacuum environments [40–48]. There are several models to explain this superlubricity; the most highly cited mechanism assumes that the hydrogen-termination of the carbon surfaces leads to little or no chemical or physical interactions during sliding contacts [48–50]. However, the superlow COF cannot be maintained in humidity conditions and COF generally increases as the water vapor pressure rises, regardless of the chemistry or type of the counter friction material: a-C:H film [47–49,51,52], steel [41,45,53–63] or ceramics [40,57,61,64–67].

When the counter material is a-C:H film itself, it was found that the rubbed surfaces contain large amounts of C–O and C=O bonded species, in addition to C–C and C–H. It was believed that tribochemical reactions take place between the carbon films and the water molecules, resulting in oxygen- and/or hydroxyl-terminated surfaces and thus leads to high COF [48]. When the counter material is steel, a transfer layer containing C, O and Fe can be found in the rubbed area, indicating that tribochemical reactions among the a-C:H film, steel surface and water are involved during the process of rubbing. This transfer layer dominates the friction and wear properties of the a-C:H/steel interface [58,68]. It was further found that adsorbed water molecules at relative low humidity act as a molecular lubricant of the oxidized DLC surface, while multilayers of water adsorbed at near-saturation act as electrolyte inducing electrochemical galvanic corrosion reactions on the steel surface (Figure 3) [63]. When the counter surface is ceramics, similar to the situation of steel, tribochemical reactions also occur during the rubbing process and the resulting transfer layer controls the friction and wear.

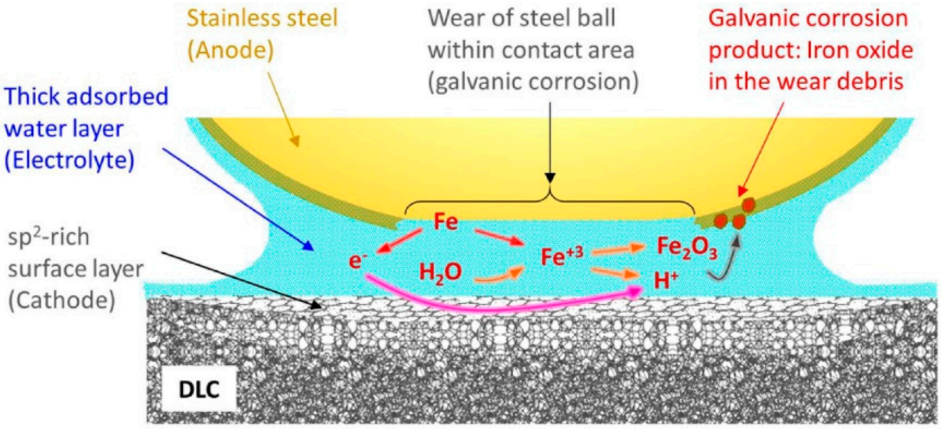

Figure 3. Schematics of the reactions among DLC films, steel surfaces and water involved in the process of rubbing [63].

Figure 3. Schematics of the reactions among DLC films, steel surfaces and water involved in the process of rubbing [63].

Since moisture has a negative effect on the friction and wear of a-C:H films, some efforts have been made to decrease the humidity dependence. The most widely used method is to produce Si-doped or Ti-doped DLC films [67–71]. The humidity dependence can be decreased with the additional elements, but superlubricity has not been achieved in ambient or humid conditions. Moreover, mechanisms for humidity tolerance effects of such doping in DLC are not fully understood.

Since moisture has a negative effect on the friction and wear of a-C:H films, some efforts have been made to decrease the humidity dependence. The most widely used method is to produce Si-doped or Ti-doped DLC films [67–71]. The humidity dependence can be decreased with the additional elements, but superlubricity has not been achieved in ambient or humid conditions. Moreover, mechanisms for humidity tolerance effects of such doping in DLC are not fully understood.

As for the a-C film, its COF in inert conditions is relatively high. However, unlike the a-C:H films, the humidity has a positive effect on the friction and wear of a-C films [49–52,55,65,72–74]. The mechanism here is very analogous to that of graphite and graphene. Water molecules can passivate the wear-induced new surface by dissociating at the dangling bond sites, thus reducing the adhesion between the sliding surfaces.

As for the a-C film, its COF in inert conditions is relatively high. However, unlike the a-C:H films, the humidity has a positive effect on the friction and wear of a-C films [49–52,55,65,72–74]. The mechanism here is very analogous to that of graphite and graphene. Water molecules can passivate the wear-induced new surface by dissociating at the dangling bond sites, thus reducing the adhesion between the sliding surfaces.

4. Ultra-Nanocrystalline Diamond (UNCD)

Diamond is also an important category of carbon material and possesses good tribological properties. However, diamond films produced at early times are of high roughness, which greatly limits the application of diamond films as lubricating coatings. Over the years, the surface roughness problem was resolved with the creation of UNCD films. The as-generated UNCD film can be very smooth [75,76] and it shows high wear-resistance. Therefore, it offers sustainable tribological properties, especially in high humid environments [77–80]. At early times, there are mainly two hypothesizes proposed to explain the humidity dependence. One is that there is a rehybridization process taking place during the rubbing

4. Ultra-Nanocrystalline Diamond (UNCD)

Diamond is also an important category of carbon material and possesses good tribological properties. However, diamond films produced at early times are of high roughness, which greatly limits the application of diamond films as lubricating coatings. Over the years, the surface roughness problem was resolved with the creation of UNCD films. The as-generated UNCD film can be very smooth [75,76] and it shows high wear-resistance. Therefore, it offers sustainable tribological properties, especially in high humid environments [77–80]. At early times, there are mainly two hypothesizes proposed to explain the humidity dependence. One is that there is a rehybridization process taking place during the rubbing process, and graphite-like structure is generated on the sliding surface and further dominates the humidity dependence of the friction and wear [81–83]. The other is that water molecules dissociate at dangling bond sites and thus passivate the sliding surfaces [75]. Both of these hypotheses were plausible. However, the existence of crystalline graphite formation on the rubbed surface of UNCD has not been confirmed [78,84,85]. Recent DFT calculations and first principles analysis predicted the dissociative passivation of dangling bonds on diamond by water [86,87]. In this way, the hypothesis of passivation becomes more accepted.

5. Transition Metal Dichalcogenides (TMDs)

TMDs are also widely used as solid lubricants for a long time. The most notable system is MoS_2. The effect of humidity on the tribological properties of MoS_2 was first reported in 1950s [88]. It was found that the friction and wear of MoS_2 increases as the environmental humidity increases, which is opposite to the trend observed for graphite and graphene. It was also found that storing MoS_2 in humid environment can increase friction and wear compared to dry storage conditions [89,90].

Based on the experimental results mentioned above, there are mainly two mechanisms proposed at the early stage. The first mechanism is that the MoS_2 surface is oxidized much more quickly in a humid environment [91–93], and the shear stress will facilitate the oxidation process [94]. X-ray photoelectron and Auger electron spectroscopy analyses showed that the sulfur is removed from the MoS_2 surface and X-ray diffraction showed the formation of MoO_3 [92]. It was also reported that H_2S is produced and released as a result of oxidation [93,95]. The second mechanism is that some of physisorbed water molecules occupy in the wedge-shape cavities of MoS_2, which increases the adhesion force between sliding interfaces [96,97].

Later, by performing tribo-tests in water-contained nitrogen and oxygen-contained nitrogen separately, Khare et al. found that water does not promote oxidation near room temperature and only oxygen induces detectable oxidation [98,99]. The absorption is reversible and the friction is strongly dependent on the amount of water in the environment, which suggests that the adsorption of water onto MoS_2 is physical rather than chemical [98,99].

It should be noted that the edge sites of MoS_2 is chemically more reactive than the basal plane. Computational simulations suggest that the MoS_2 nanosheet is a hydrophobic and low-friction surface [100], and water molecules will be dissociatively adsorbed at the MoS_2 edge site [22,101,102]. Some researchers performed AFM-based friction experiments on MoS_2 and WS_2 basal planes, but contrary conclusions on the humid dependence were put forward [103–105]. Further tests on both basal planes and edge sites are necessary.

In order to maintain the excellent lubricity of MoS_2 in humid environments, various methods have been attempted. The most common method is to use additives to make MoS_2 composite coating. Among different kinds of additives, doping with metals such as Ti, Pb, Au, Cr, Cu, and Zr are found to offer some improved humid tolerance [106–117]. Making composites with PTFE [118] and WC [119] were also claimed to improve the tribological properties of the coating. Meanwhile, it was also reported that if the crystalline order of the coating is increased, the humid resistance could be improved [120–122]. This phenomenon is also suggestive that the edge sites play an important role in the humidity dependence. Moreover, it was reported that the friction and wear of $MoSe_2$ and WSe_2 are hardly influenced by ambient humidity [123,124]. The chemistry of disulfide and diselenide materials in humid environments appear to be drastically different.

6. Boron-Based Materials

h-BN is another two-dimensional layered material used as solid lubricant coating. It is isoelectronic to graphene. The effect of humidity on the tribological properties of h-BN was first reported in 1960s [9]. It was found that the friction of h-BN decreases as the water vapor pressure increases [9,125], which is similar to that of graphite and graphene. However, very limited papers discussed the mechanism of h-BN humidity dependence. Molecular dynamics simulations have shown that monolayer BN sheets are weakly hydrophobic with nearly the same water contact angle as graphene [126]. Considering this similarity, it was speculated that the mechanism of the humidity dependence of friction is similar for graphene and h-BN.

Boric acid has a layered triclinic crystal structure and is well known to give ultra-low COF when used as a solid lubricant in air. It was proposed that a layer of lubricous boric acid can be generated during the sliding due to the reaction between boric oxide coatings and surrounding moisture [127–133]. However, a contradictory explanation was put forward since the films formed on boron oxide showed no evidence of crystalline structure [134]. As for the boric acid itself, its tribological properties are highly dependent on environmental humidity. It was found that, in dry condition, when boric acid is rubbed with a stainless steel ball, the friction is high and the boric acid suffers catastrophic wear [135]. Moreover, it was proved through vibrational spectroscopy that the lubricating vapor molecules barely absorb on the basal plane, but may absorb onto the edge sites of boric acid [135].

On comparing these experimental data and literature with the humidity dependence of graphite, TMDs, h-BN and boric acid lubrication, a mechanism was proposed, explaining how the reaction of edge sites of layered materials with water and other molecules can affect the inter-layer shear along the basal plane (Figure 4) [135].

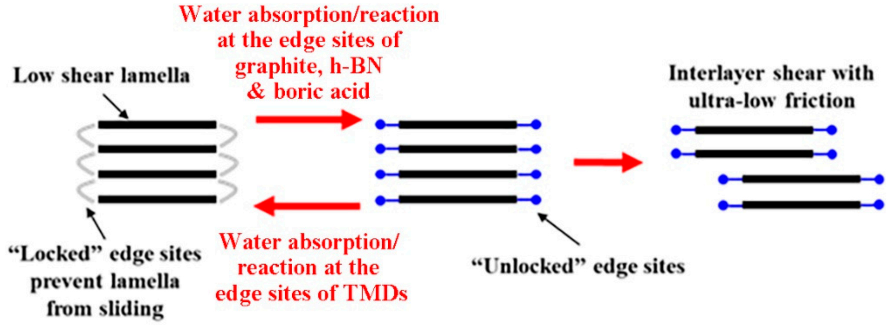

Figure 4. Schematics of the mechanism of humidity dependent friction behavior of graphite, TMDs, h-BN and boric acid.

7. Silicon and Silicon Oxides

Monocrystalline silicon is the most widely used substrate and structural material in integrated circuits and micro-electromechanical systems (MEMS) [136–138]. The friction and wear mechanisms of silicon in humid air are vital in determining the reliability and durability of dynamic MEMS devices [139–142]. Due to the oxidation reaction with oxygen and water in air, the bare silicon surface exposed to air for a long time is normally covered by a layer of native oxide (SiO_x), with typical thickness of <2 nm. The growth of the SiO_x layer changes surface wettability and chemical reactivity, and further significantly affects the humidity dependence of tribological properties (i.e., adhesion, force, and wear) of silicon [143].

The water adsorption behaviors of hydrogen-terminated Si-H surface and native oxide (SiO_x) surface are drastically different. The former is hydrophobic (with a water contact angle of 83°) [144], while the latter is hydrophilic (with a water contact angle of 0°), especially when its surface is terminated with hydroxyl (OH) groups [145]. Figure 5 displays the infrared spectra of water layers adsorbed on the hydrophilic Si–OH and hydrophobic Si–H surfaces and the average thickness of the adsorbed water layer calculated from infrared absorption band intensity [145]. On the hydrophilic surface, the peak corresponding to a strongly hydrogen-bonded solid-like (or more ordered) structure is dominant at low humidity and the peak corresponding to a liquid-like (or disordered) structure grows as humidity approaches the saturation point [146]. In contrast, on the hydrophobic Si–H surface, the liquid-like while the latter is hydrophilic (with a water contact angle of 0°), especially when its surface is terminated with hydroxyl (OH) groups [145]. Figure 5 displays the infrared spectra of water layers adsorbed on the hydrophilic Si–OH and hydrophobic Si–H surfaces and the average thickness of the adsorbed water layer calculated from infrared absorption band intensity [145]. On the hydrophilic surface, the peak corresponding to a strongly hydrogen-bonded solid-like (or more ordered) structure is dominant at low humidity and the peak corresponding to a liquid-like (or disordered) structure grows as humidity approaches the saturation point [146]. In contrast, on the hydrophobic Si–H surface, the liquid-like component is always dominant. The average thickness of the adsorbed water layer is less than one molecular layer on the Si–H surface, while it reaches up to four layers on the Si–OH surface.

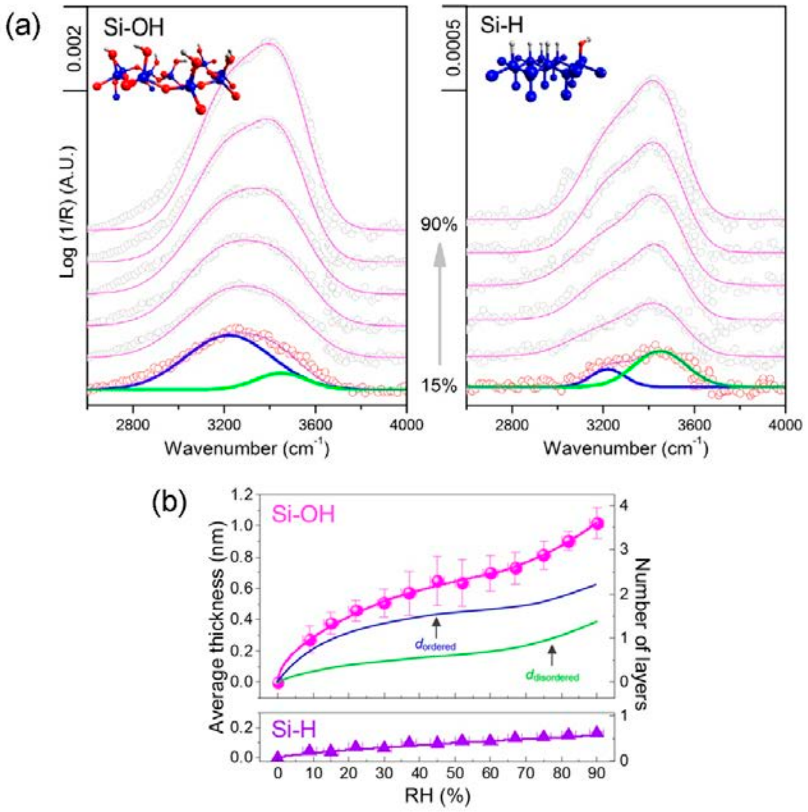

Figure 5. (**a**) ATR-IR spectra of the O–H stretching region of water adsorbed on Si–OH and Si–H surfaces at RHs of 15%, 30%, 45%, 60%, 75%, and 90%. The insets schematically show the Si–OH functional groups on a native oxide layer and the Si–H groups on the HF-etched surface. Si, blue; O, red; H, gray. The O–H stretching region is fitted with two components: strongly H-bonded water (blue lines centered at 3200–3275 cm^{-1}) and weakly H-bonded water (green lines centered at 3400–3450 cm^{-1}). (**b**) Adsorption isotherm of adsorbed water on hydrophilic Si–OH and hydrophobic Si–H surfaces [145].

In macroscopic tribo-test conditions, the adsorbed water layers tend to have detrimental effects [147,148]. Figure 6 compares the wear tracks made in three different environmental conditions: Dry nitrogen, humid nitrogen, and nitrogen with *n*-pentanol vapor [147]. In dry condition, the center area of the wear track is relatively flat and there are some piles of debris at the sides. As for the wear track generated in humid condition, there are deep scratch lines running along the sliding direction, but there is not much debris at the sides. It is believed that the cylindrical wear particles generated in dry condition leads to a third body rolling contact condition, which may result in low friction [147]. The adsorbed water molecules facilitate tribochemical reaction at the tribological interface and aggravate wear of the silicon substrate. The detrimental effect of water adsorption on wear of silicon can be seen clearly when it is compared with the beneficial effect of n-pentanol

---

Figure 5. (**a**) ATR-IR spectra of the O–H stretching region of water adsorbed on Si–OH and Si–H surfaces at RHs of 15%, 30%, 45%, 60%, 75%, and 90%. The insets schematically show the Si–OH functional groups on a native oxide layer and the Si–H groups on the HF-etched surface. Si, blue; O, red; H, gray. The O–H stretching region is fitted with two components: strongly H-bonded water (blue lines centered at 3200–3275 cm^{-1}) and weakly H-bonded water (green lines centered at 3400–3450 cm^{-1}). (**b**) Adsorption isotherm of adsorbed water on hydrophilic Si–OH and hydrophobic Si–H surfaces [145].

In macroscopic tribo-test conditions, the adsorbed water layers tend to have detrimental effects [147,148]. Figure 6 compares the wear tracks made in three different environmental conditions: Dry nitrogen, humid nitrogen, and nitrogen with *n*-pentanol vapor [147]. In dry condition, the center area of the wear track is relatively flat and there are some piles of debris at the sides. As for the wear track generated in humid condition, there are deep scratch lines running along the sliding direction, but there is not much debris at the sides. It is believed that the cylindrical wear particles generated in dry condition leads to a third body rolling contact condition, which may result in low friction [147]. The adsorbed water molecules facilitate tribochemical reaction at the tribological interface and aggravate wear of the silicon substrate. The detrimental effect of water adsorption on wear of silicon can be seen clearly when it is compared with the beneficial effect of n-pentanol adsorption in the same mechanical test condition (Figure 6). The tribochemical wear of Si/SiO$_2$ tribo-pair appear to be a three-step process [149–152]. The initial appearance of Si–OH groups is caused by chemical reactions of Si–H groups with water molecules impinging from the vapor phase. The Si–OH group of the substrate surface can undergo condensation reactions with the Si–OH group of the counter-surface, forming a Si–O–Si bridge between two solid surfaces. The rupture of underlying Si-Si bonds will lead to wear of materials.

adsorption in the same mechanical test conditions (Figure 6). The tribochemical wear of Si/SiO_2 tribo-pair appear to be a three-step process [149–152]. The initial appearance of Si–OH groups is caused by chemical reactions of Si–H groups with water molecules impinging from the vapor phase. The Si–OH group of the substrate surface can undergo condensation reactions with the Si–OH group of the counter-surface, forming a Si–O–Si bridge between two solid surfaces. The rupture of underlying Si-Si bonds will lead to wear of materials.

Lubricants 2018, 6, x FOR PEER REVIEW 9 of 27

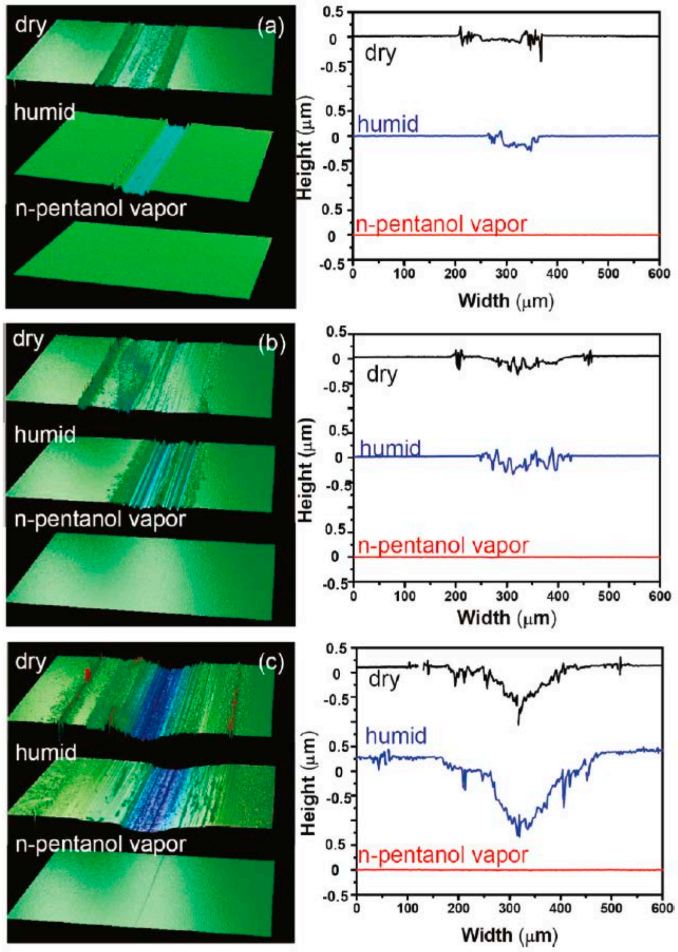

Figure 6. Optical profilometry images and characteristic line profiles of wear tracks made in dry, 50% RH, and 50% P/P_{sat} *n*-pentanol vapor environments with an applied load of (**a**) 0.1, (**b**) 0.3, and (**c**) 0.7 N [147].

Figure 6. Optical profilometry images and characteristic line profiles of wear tracks made in dry, 50% RH, and 50% P/P_{sat} *n*-pentanol vapor environments with an applied load of (**a**) 0.1, (**b**) 0.3, and (**c**) 0.7 N [147].

DFT calculations for the Si–O–Si bond dissociation via reactions with water molecules impinging on the substrate revealed that the activation energy for this reaction is lowered when the substrate surface is terminated with hydroxyl groups [147]. Molecule dynamics (MD) simulation also shows that tribochemical reactions, which involve the formation of covalent bonds bridging two solid surfaces, vary depending on the amount of interfacial water molecules, contact pressure and system temperature [153,154]. Higher values of these parameters can cause more Si atoms to be removed due to the formation of an increased number of interfacial Si–O–Si bridge bonds.

However, when the amount of interfacial water molecules is large enough to form multilayers of physisorbed water, the degree of bridge bond formation is substantially reduced since the silicon atoms at the sliding interface are physically separated due to thick water layers [154,155]. Some studies also show that the friction between Si_3N_4 ball and silicon substrate begin to decrease when humidity is higher than 80% RH, which is mainly attributed to the formation of an adsorbate film acting as a boundary lubricant that separates the two surfaces from each other, thereby hindering bond formation and leading to lower friction [156,157].

As the dimension of the sliding contact shrinks to nanoscale, the effects of surface chemistry and adsorbed water layer are manifested in more complicated ways. In AFM experiments, both Si–H and

DFT calculations for the Si–O–Si bond dissociation via reactions with water molecules impinging on the substrate revealed that the activation energy for this reaction is lowered when the substrate surface is terminated with hydroxyl groups [147]. Molecule dynamics (MD) simulation also shows that tribochemical reactions, which involve the formation of covalent bonds bridging two solid surfaces, vary depending on the amount of interfacial water molecules, contact pressure and system temperature [153,154]. Higher values of these parameters can cause more Si atoms to be removed due to the formation of an increased number of interfacial Si–O–Si bridge bonds.

However, when the amount of interfacial water molecules is large enough to form multilayers of physisorbed water, the degree of bridge bond formation is substantially reduced since the silicon atoms at the sliding interface are physically separated due to thick water layers [154,155]. Some studies also show that the friction between Si_3N_4 ball and silicon substrate begin to decrease when humidity is higher than 80% RH, which is mainly attributed to the formation of an adsorbate film acting as a boundary lubricant that screens the two surfaces from one another, thereby hindering bond formation and leading to lower friction [156,157].

As the dimension of the sliding contact shrinks to nanoscale, the effects of surface chemistry and adsorbed water layer are manifested in more complicated ways. In AFM experiments, both Si–H and SiO$_x$ surfaces show excellent wear resistance in dry condition, when the applied shear stress is lower than the yield stress of the substrate, regardless of counter-surface materials (active SiO$_2$ and inert diamond) [158–162]. As humidity increases, wear occurs on Si–H and SiO$_x$ surfaces when the counter surface is SiO$_2$, but wear is negligible when the counter surface is diamond at the same loading conditions. These results suggest that the chemistry of the counter surface (SiO$_2$ vs. diamond) plays an important role in the wear of materials [163]. On the Si–H surface, as humidity increases, friction decreases monotonically, but wear increases initially, reaches a maximum value, and then eventually decreases [161,162,164]. In contrast, on the SiO$_x$ surface, both friction and wear first increase to a maximum value at 50% RH and then decrease below the detection limit of AFM at RH above 85% or in water (Figure 7a) [163,165–171]. It is also noted that the effect of humidity on wear of SiO$_x$-covered Si wafer varies depending on the sliding speed (Figure 7b) [168].

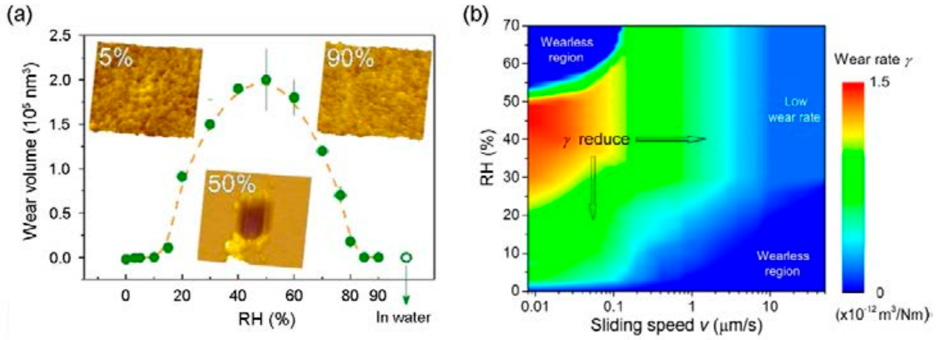

Figure 7. (**a**) Effect of RH on the wear volume V on silicon surface with native oxide layer. The insets are AFM images of wear scars on silicon surface at various RHs. F_n = 3 μN, L = 200 nm, v = 2 μm/s, and N = 200 cycles [166]. (**b**) Nanowear map of the single crystalline silicon surface scratched with a SiO$_2$ sphere (radius = 1 μm) at an applied load of 3 μN for 100 reciprocating cycles [168].

If the aforementioned hypothesis of the involvement of Si–O–Si bridge bond formation is adapted [162–164,166,168,169], it implies that interfacial bridge bond formation may be affected by the structure and thickness of the adsorbed water film. On the basis of typical silicon oxide structures, the distance between two Si atoms connected via the Si–O–Si covalent bond bridge is estimated to be around 0.324 nm [172], comparable to the thickness of one layer of molecular water. As several layers of water grow on the surface at high RH conditions, the probability for the asperities to come close enough to form Si–O–Si bridges decreases [166]. Finally, when the thickness of adsorbed water film on the silicon surface exceeds a few nanometers at RH > 85% [173], the probability for the Si–O–Si bridge formation becomes very low.

In solid contact mechanics, the friction force is normally proportional to the contact area and the proportionality constant corresponds to the shear stress of the contact [174,175]. However, in humid environment, solid contact mechanics cannot fully explain the humidity dependence of friction. Figure 8 plots friction force (F_t) between the native oxide (SiO$_x$) layer and the silica surface (SiO$_2$) as a function of water meniscus area (A_m) and volume (V_m) estimated from a thermally activated water-bridge formation model [165]. It was found that Ft correlates linearly with V_m, but not with A_m at RH < 50%; and then its V_m dependence becomes weaker as RH increases above 50%. Considering the water adsorption isotherm shown in Figure 5, it appears that the solid-like water layer structure formed on the silica surface plays a critical role in friction at RH < 50% and its significance diminishes at RH ≥ 50% [146,165,176,177].

Lubricants **2018**, *6*, x FOR PEER REVIEW 10 of 27

SiO$_x$ surfaces show excellent wear resistance in dry condition, when the applied shear stress is lower than the yield stress of the substrate, regardless of counter-surface materials (active SiO$_2$ and inert diamond) [158–162]. As humidity increases, wear occurs on Si–H and SiO$_x$ surfaces when the counter surface is SiO$_2$, but wear is negligible when the counter surface is diamond at the same loading conditions. These results suggest that the chemistry of the counter surface (SiO$_2$ vs. diamond) plays an important role in the wear of materials [163]. On the Si–H surface, as humidity increases, friction decreases monotonically, but wear increases initially, reaches a maximum value, and then eventually decreases [161,162,164]. In contrast, on the SiO$_x$ surface, both friction and wear first increase to a maximum value at 50% RH and then decrease below the detection limit of AFM at RH above 85% or in water (Figure 7a) [163,165–171]. It is also noted that the effect of humidity on wear of SiO$_x$-covered Si wafer varies depending on the sliding speed (Figure 7b) [168].

Figure 7. (**a**) Effect of RH on the wear volume V on silicon surface with native oxide layer. The insets are AFM images of wear scars on silicon surface at various RHs. F_n = 3 μN, L = 200 nm, v = 2 μm/s, and N = 200 cycles [166]. (**b**) Nanowear map of the single crystalline silicon surface scratched with a SiO$_2$ sphere (radius = 1 μm) at an applied load of 3 μN for 100 reciprocating cycles [168].

If the aforementioned hypothesis of the involvement of Si–O–Si bridge bond formation is adapted [162–164,166,168,169], it implies that interfacial bridge bond formation may be affected by the structure and thickness of the adsorbed water film. On the basis of typical silicon oxide structures, the distance between two Si atoms connected via the Si–O–Si covalent bond bridge is estimated to be around 0.324 nm [172], comparable to the thickness of one layer of molecular water. As several layers of water grow on the surface at high RH conditions, the probability for the asperities to come close enough to form Si–O–Si bridges decreases [166]. Finally, when the thickness of adsorbed water film on the silicon surface exceeds a few nanometers at RH > 85% [173], the probability for the Si–O–Si bridge formation becomes very low.

In solid contact mechanics, the friction force is normally proportional to the contact area and the proportionality constant corresponds to the shear stress of the contact [174,175]. However, in humid environment, solid contact mechanics cannot fully explain the humidity dependence of friction. Figure 8 plots friction force (F_t) between the native oxide (SiO$_x$) layer and the silica surface (SiO$_2$) as a function of water meniscus area (A_m) and volume (V_m) estimated from a thermally activated water-bridge formation model [165]. It was found that Ft correlates linearly with V_m, but not with A_m at RH < 50%; and then its V_m dependence becomes weaker as RH increases above 50%. Considering the water adsorption isotherm shown in Figure 5, it appears that the solid-like water layer structure formed on the silica surface plays a critical role in friction at RH < 50% and its significance diminishes at RH ≥ 50% [146,165,176,177].

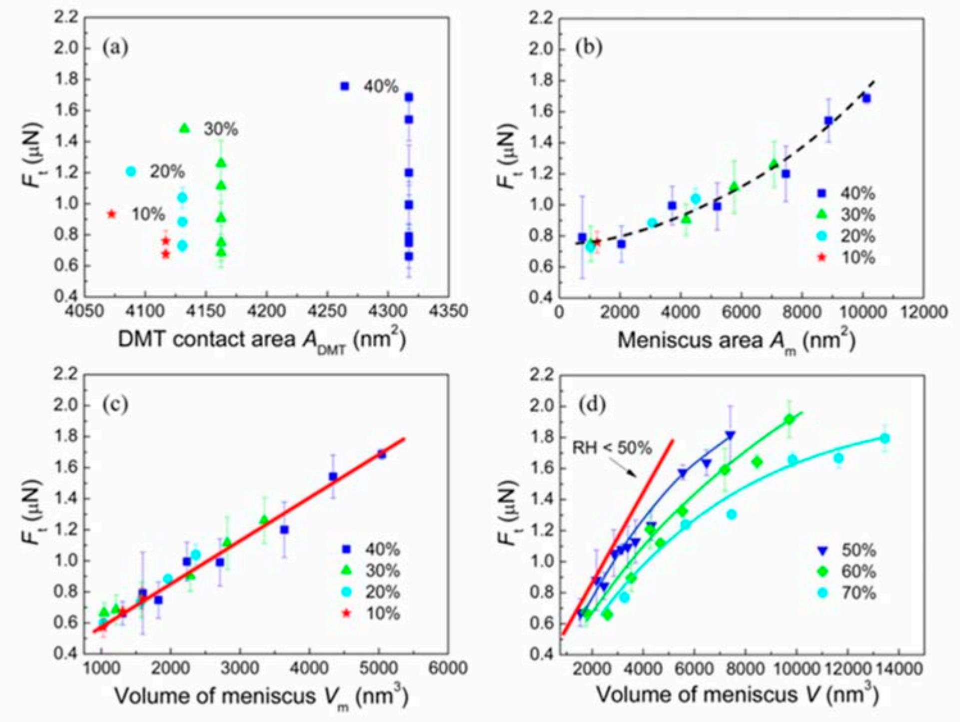

Figure 8. Friction force F_t versus (**a**) DMT contact area (A_{DMT}); (**b**) meniscus area (A_m); (**c**) meniscus volume (V_m) for the contact between the SiO$_x$ surface and the silica microsphere (F_n = 2 μN) moving at various sliding speed in RH < 50%. (**d**) F_t versus V_m for the high RH regime (≥50%) [165].

Figure 8. Friction force F_t versus (a) DMT contact area (A_{DMT}) (b) meniscus area (A_m) (c) meniscus volume (V_m) for the contact between the SiO$_x$ surface and the silica microsphere (F_n = 2 μN) moving at various sliding speed in RH < 50%. (d) F_t versus V_m for the high RH regime (≥50%) [165].

The fact that only the atoms exposed at the top most surface can be involved in tribochemical reactions with molecules adsorbed from the gas phase can provide extreme precision in nanofabrication. As shown in Figure 9, Chen et al. utilized that attribute of water-induced tribochemical reactions and demonstrated the removal of single atomic layer at a time on a silicon wafer surface using AFM [178]. Since AFM was used, any arbitrary shape of patterns with the control of etch depth at any given atomic layer could be possible. This opens a new opportunity or potential of utilizing tribochemical etching for nanomanufacturing.

The fact that only the atoms exposed at the top most surface can be involved in tribochemical reactions with molecules adsorbed from the gas phase can provide extreme precision in nanofabrication. As shown in Figure 9, Chen et al. utilized that attribute of water-induced tribochemical reactions and demonstrated the removal of single atomic layer at a time on a silicon wafer surface using AFM [178]. Since AFM was used, any arbitrary shape of patterns with the control of etch depth at any given atomic layer could be possible. This opens a new opportunity or potential of utilizing tribochemical etching for nanomanufacturing.

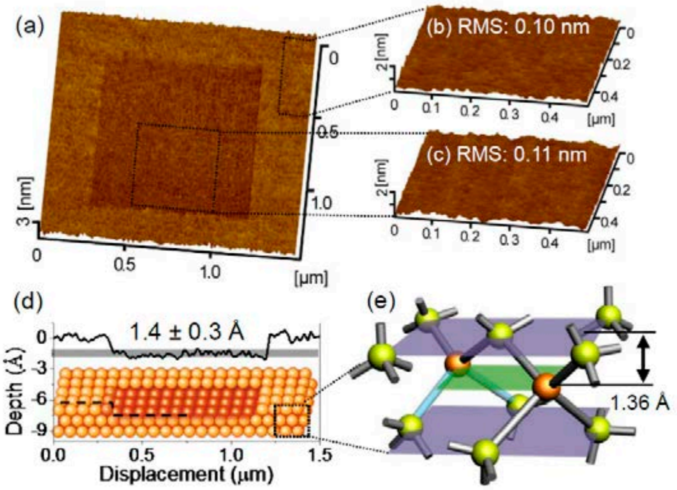

Figure 9. Single atomic layer removal of Si material. (**a**) SPM image (1.5 μm × 1.5 μm) of the manufactured area. Topographic images (0.5 μm × 0.5 μm) of (**b**) the original surface, and (**c**) the manufactured surface. (**d**) Cross-section profile of the manufactured area corresponding to the single atomic layer removal on Si (100). (**e**) Crystal structure of Si (100) [178].

Figure 9. Single atomic layer removal of Si material. (a) SPM image (1.5 μm × 1.5 μm) of the manufactured area. Topographic images (0.5 μm × 0.5 μm) of (b) the original surface, and (c) the manufactured surface. (d) Cross-section profile of the manufactured area corresponding to the single atomic layer removal on Si (100). (e) Crystal structure of Si (100) [178].

8. Silicates

Although the main constituent of silicate glass is silicon oxide, the wear behavior of multicomponent silicate glasses is quite different from that of pure silica surface. At low load conditions where mechanical damage could be prevented, wear of silicate glass surfaces occurs via mechanochemical processes [179,180]. In the glass field, it is well known that the crack propagation velocity is greatly enhanced as

8. Silicates

Although the main constituent of silicate glass is silicon oxide, the wear behavior of multicomponent silicate glasses is quite different from that of pure silica surface. At low load conditions where mechanical damage could be prevented, wear of silicate glass surfaces occurs via mechanochemical processes [179,180]. In the glass field, it is well known that the crack propagation velocity is greatly enhanced as humidity increases [181–183]. This behavior is explained well with the stress corrosion theory, which dictates that water can facilitate the dissociation of the Si–O–Si bond under tensile stress [181–185]. If the same principle pertained to the wear of silicate glass under tribological conditions, then one would expect that mechanochemical wear increases as humidity increases. In a series of studies with various types of silicate glasses, it was found that sodium calcium silicate (also called soda lime silica, SLS) exhibits a peculiar RH dependence of the mechanochemical wear [186]. Figure 10 compares the cross-section line profiles of the wear tracks created at difference glass surfaces at the same contact load and sliding speed at 20%, 40%, and 90% RH conditions. In the case of fused quartz, borosilicate (BF33), boroaluminosilicate (AF45), and aluminosilicate glasses, the glass substrate wear increases as RH is raised. In contrast, the SLS glass shows very little wear in the near saturation RH condition [148,179,180,186–193]. The humidity dependences of wear of fused quartz, borosilicate, boroaluminosilicate, and aluminosilicate glasses appear to be consistent with the prediction from the stress corrosion theory; however, the wear resistance of SLS glass at near-saturation humidity defies the conventional stress corrosion theory.

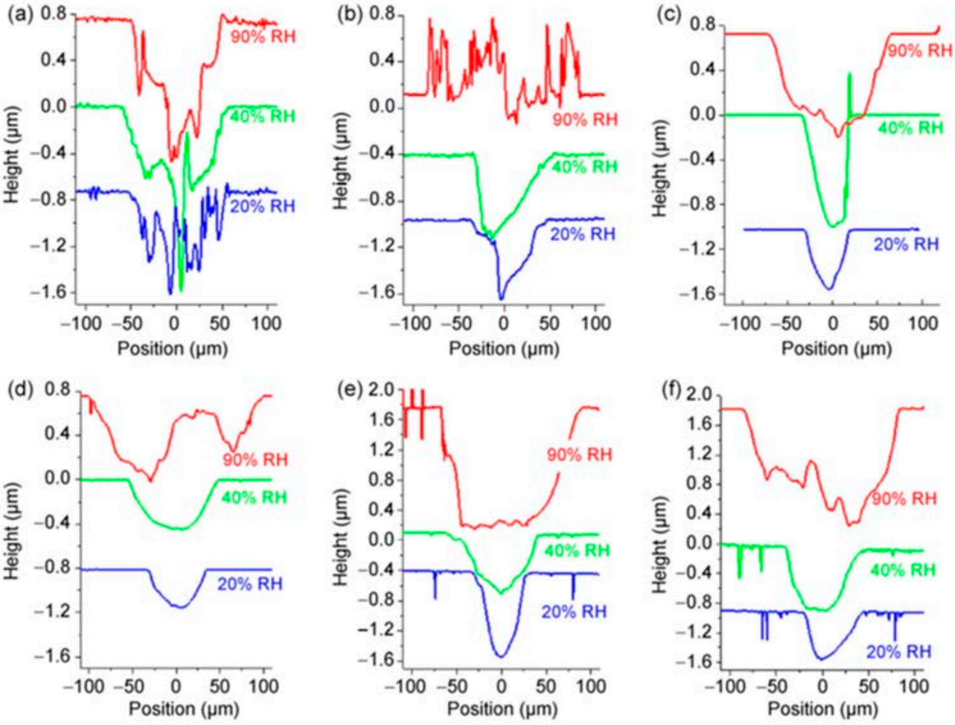

Figure 10. Line profiles of the wear tracks on different glasses under different humidity conditions: **(a)** fused quartz [186]; **(b)** soda-lime silicate glass [186]; **(c)** BF33 [179]; **(d)** AF45 [179]; **(e)** sodium aluminosilicate [187]; **(f)** K-exchanged aluminosilicate [187]. Details of tribo-test conditions can be found in the cited references.

Figure 10. Line profiles of the wear tracks on different glasses under different humidity conditions: (a) fused quartz [186]; (b) soda-lime silicate glass [186]; (c) BF33 [179]; (d) AF45 [179]; (e) sodium aluminosilicate [187]; (f) K-exchanged aluminosilicate [187]. Details of tribo-test conditions can be found in the cited references.

It was speculated that the structures of water at the surface and in the subsurface region, which are determined or affected by the presence of leachable Na^+ ions and types of silicate network, play critical roles in the observed behavior. Among the glasses tested in Figure 10 [179,180,186–194], it is noted that only SLS has leachable Na^+ ions associated with the non-bridging oxygen ($Si–O^-$; NBO) atoms in the glass network. This raises questions about the effects of Na^+ itself in the silicate network versus the structure and reactivity of adsorbed water, which may vary with Na^+ leaching. When the SLS glass surface is thermally poled, the Na^+-depleted surface (anode-side) loses the wear resistance at 90% RH, while the Na^+-accumulated surface (cathode-side) exhibits an enhanced resistance [190]. When the subsurface Na^+ ions are depleted via reaction with steam at 150–200 °C, the SLS glass loses the wear resistance at 90% RH [194]. The AF45 glass contains a trace amount of Na^+ ions in the bulk; those Na^+ ions can be pushed

It was speculated that the structures of water at the surface and in the subsurface region, which are determined or affected by the presence of leachable Na^+ ions and types of silicate network, play critical roles in the observed behavior. Among the glasses tested in Figure 10 [179,180,186–194], it is noted that only SLS has leachable Na^+ ions associated with the non-bridging oxygen ($Si–O^-$; NBO) atoms in the

glass network. This raises questions about the effects of Na^+ itself in the silicate network versus the structure and reactivity of adsorbed water, which may vary with Na^+ leaching. When the SLS glass surface is thermally poled, the Na^+-depleted surface (anode-side) loses the wear resistance at 90% RH, while the Na^+-accumulated surface (cathode-side) exhibits an enhanced resistance [190]. When the subsurface Na^+ ions are depleted via reaction with steam at 150–200 °C, the SLS glass loses the wear resistance at 90% RH [194]. The AF45 glass contains a trace amount of Na^+ ions in the bulk; those Na^+ ions can be pushed to the surface via thermal poling. The accumulation of subsurface Na^+ ions would be accompanied by the production of NBO sites for charge compensations. The Na^+-enriched AF45 glass surface also exhibits a good wear resistance at 90% RH [192].

In the past, the structure of water layers adsorbed on multicomponent glass surfaces in humid air was assumed to be the same as (at least, similar to) that on pure silica surface. That was because spectroscopic technique was not available to selectively probe water layers adsorbed on multicomponent glass in equilibrium with the humid air. However, recent study on vibrational sum frequency generation (SFG) spectroscopy (Figure 11) showed that such assumption is not correct [195,196]. The SFG spectral features of water layers on the SLS and calcium aluminosilicate (E-glass in Figure 11) glass surfaces are drastically different from those on the fused quartz surface. It is not only the glass composition, but also the surface treatment history that leads to alteration of the adsorbed water layer structure. This implies that wear mechanisms of silicate glass in humid air could be different from those of silica because the structure of the adsorbed water layer and dynamics of water molecules in the adsorbed layer are different.

structure of the adsorbed water layer and the dynamics of water molecules in the adsorbed layer are different.

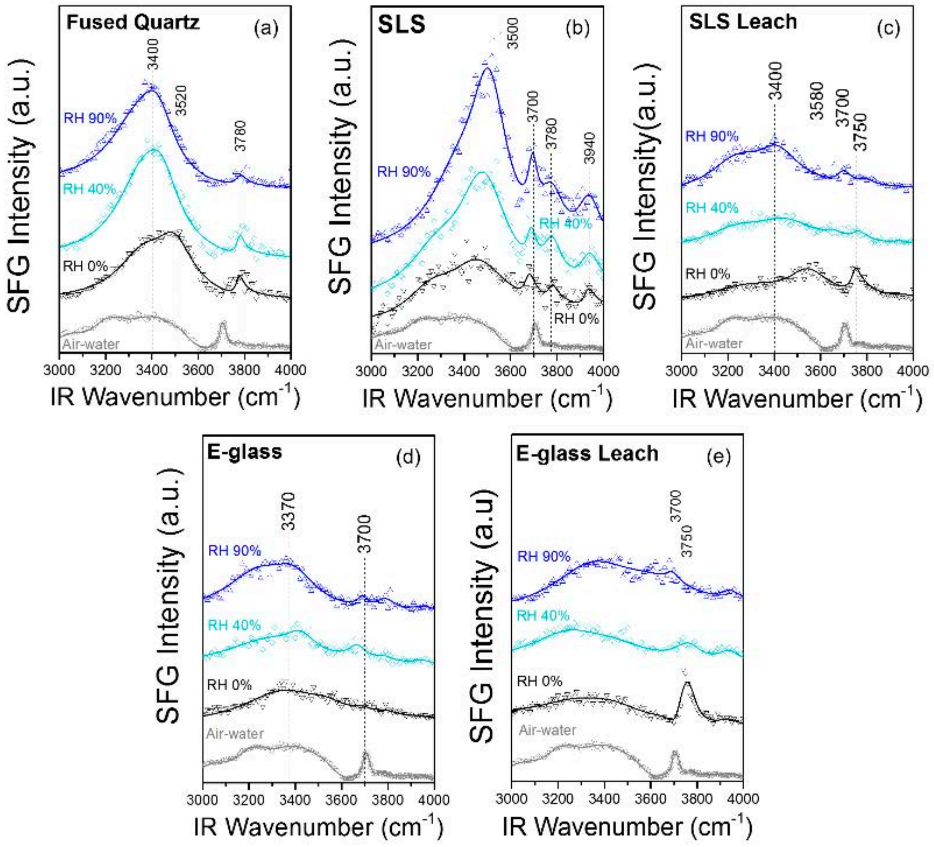

Figure 11. SFG spectra of water layers adsorbed on (**a**) fused quartz, (**b**) annealed SLS, (**c**) acid-leached SLS, (**d**) annealed E-glass, (**e**) acid-leached E-glass at RH = 0%, 40%, and 90% at room temperature [196].

Figure 11. SFG spectra of water layers adsorbed on (a) fused quartz, (b) annealed SLS, (c) acid-leached SLS, (d) annealed E-glass, (e) acid-leached E-glass at RH = 0%, 40%, and 90% at room temperature [196].

It is not only substrate chemistry and humidity, but also counter surface chemistry that plays critical roles. This appeared to counter-act the stress corrosion effect. Figure 12 shows the wear volume

It is not only substrate chemistry and humidity, but also counter surface chemistry that plays critical roles. This appeared to counter-act the stress corrosion effect. Figure 12 shows the wear volume of SLS

glass measured after AFM scratch test in different conditions [197]. When the diamond tip is used as a counter surface for scratch, a protrusion of substrate surface (often called hillock) is observed at low contact pressures. The material removal (which is consistent with the surface damage pattern of 'wear' process) is observed at the contact pressure above the yield point of SLS glass. When humidity is introduced during the scratch with the diamond tip, the critical contact pressure for the wear process is reduced from 3.5 GPa in the vacuum condition to about 2 GPa. This reduction might be attributed to (at of SLS glass measured after AFM scratch test in different conditions [197]. When the diamond tip is used as a counter surface for scratch, a protrusion of substrate surface (often called hillock) is observed at low contact pressures. The material removal (which is consistent with the surface damage pattern of 'wear' process) is observed at the contact pressure above the yield point of SLS glass. When humidity is introduced during the scratch with the diamond tip, the critical contact pressure for the wear process is reduced from 3.5 GPa in the vacuum condition to about 2 GPa. This reduction might be attributed to (at least, consistent with) the stress corrosion process involving adsorbed water molecules in tribochemical reactions. When the diamond tip is replaced with a silica sphere in the same condition, the critical contact pressure for wear is further reduced to about 0.7 GPa. This implies that the silanol groups at the counter surface are actively involved in the tribochemical wear of the SLS glass surface.

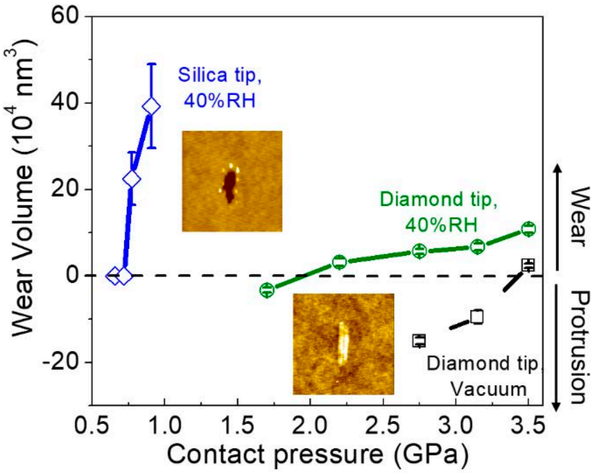

Figure 12. Effect of contact pressure on the wear volume of SLS glass by various RH and counter-surface materials. The negative wear volume is surface protrusion (hillock) and the positive volume is material removal. The insets are AFM image and characteristic line profile of nanowear track at SLS glass [197].

In tribology, the wear process is often explained with the Archard wear equation or the Reye–Archard-Khrushchov wear law, which predicts that the wear volume is determined by the hardness of the softest contacting surfaces [198,199]. This relationship considers mechanical properties only; thus, it may work well in dry or inert conditions, but not in humid air. Figure 13 displays the wear images of SLS glass substrates rubbed with Si_3N_4 ball, Al_2O_3 ball, and 440C stainless steel balls in 20%, 40%, and 90% RH conditions [188]. In the dry condition (not shown in Figure 13), the SLS glass surface is badly worn (with 5–10 μm deep scratch marks), because its hardness is much lower than the hardness of the ball material [188]. However, in humid conditions, the damage to the softer SLS glass surface is very small; instead, the surfaces of the harder ball materials are polished. These results clearly indicate that the wear behavior of materials in humid air cannot be explained with the mechanical properties of materials involved in tribological contacts. The surface chemistry, more accurately tribochemistry, of materials in the given test condition play dominant roles.

Figure 12. Effect of contact pressure on the wear volume of SLS glass by various RH and counter-surface materials. The negative wear volume is surface protrusion (hillock) and the positive volume is material removal. The insets are AFM image and characteristic line profile of nanowear track at SLS glass [197].

In tribology, the wear process is often explained with the Archard wear equation or the Reye–Archard-Khrushchov wear law, which predicts that the wear volume is determined by the hardness of the softest contacting surfaces [198,199]. This relationship considers mechanical properties only; thus, it may work well in dry or inert conditions, but not in humid air. Figure 13 displays the wear images of SLS glass substrates rubbed with Si_3N_4 ball, Al_2O_3 ball, and 440C stainless steel balls in 20%, 40%, and 90% RH conditions [188]. In the dry condition (not shown in Figure 13), the SLS glass surface is badly worn (with 5–10 μm deep scratch marks), because its hardness is much lower than the hardness of the ball material [188]. However, in humid conditions, the damage to the softer SLS glass surface is very small; instead, the surfaces of the harder ball materials are polished. These results clearly indicate that the wear behavior of materials in humid air cannot be explained with the mechanical properties of materials involved in tribological contacts. The surface chemistry, more accurately tribochemistry, of materials in the given test condition play dominant roles.

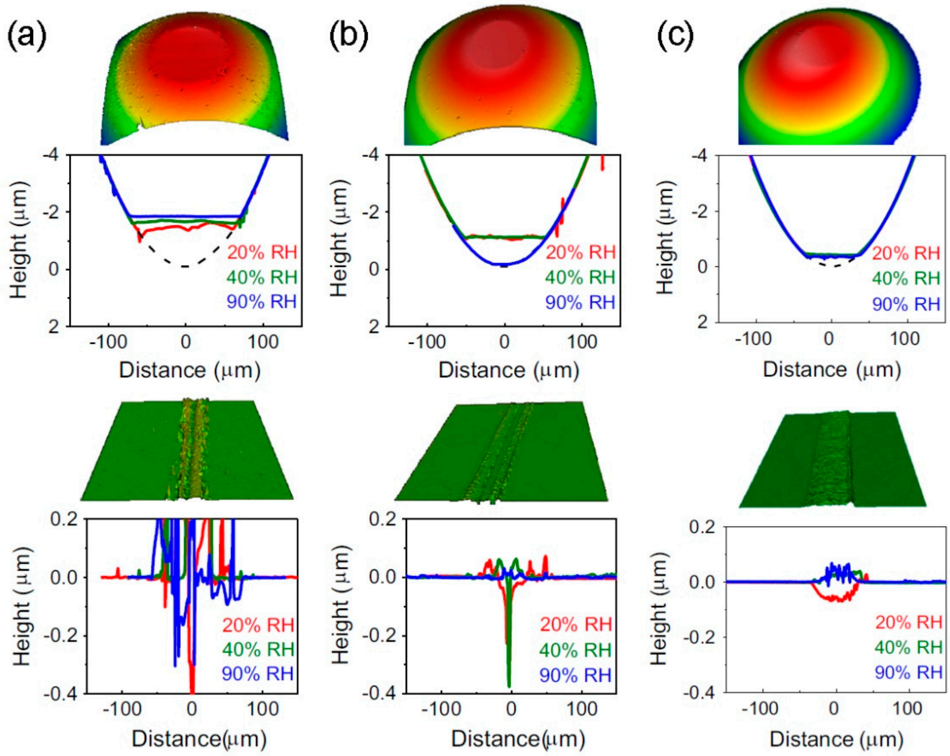

Figure 13. Characteristic optical profilometry images at 40% RH and line profiles of various balls surface (upper) and soda-lime-silica glass substrates (lower) after 400 cycles of scratching at an applied load of 0.2 N under 20%, 40%, and 90% humidity conditions. (a) Si_3N_4 ball. (b) Al_2O_3 ball, and (c) 440C stainless steel ball [188].

9. Advanced Ceramics

High hardness and mechanical strength of advanced ceramics are traits that make them suitable for tribo-materials [200,201]. Among various types of advanced ceramics, the tribological properties of Al_2O_3, Si_3N_4, SiC and ZrO_2 are studied most extensively [200–212]. The wear mechanisms of these advanced ceramics can be categorized into three main types: (i) Mechanical fracture under high stress; (ii) wear debris induced third-body abrasion; and (iii) material removal due to tribochemical reactions [201]. The mild wear mainly takes place by fine wear debris and tribochemistry, while the severe wear happens with relative large size wear debris due to mechanical cracking and subsequent abrasion [200,201].

The investigation of effect of humidity on tribological properties of advanced ceramics mainly started in 1980s. Generally, when advanced ceramics are tested in unlubricated conditions, friction and wear decrease as environmental humidity increases [213–226]. It was found that the worn surface in low humidity conditions is rough, but it is relatively smoother in high humidity conditions due to tribochemical reactions involving the adsorbed water molecules. For Al_2O_3 surfaces, the main tribochemical reaction product is $Al(OH)_3$ [219,220,227]. For Si_3N_4 and SiC surfaces, the main products are SiO_2 and $Si(OH)_4$ [213–216,228–231]. It was believed that these hydroxide species are lubricious and could work as a protective or sacrificial layer to prevent the substrate from further wear. Therefore, the wear mechanism appears to gradually change from mechanical to tribochemical as environmental humidity increases. It may also explain why the degradation behavior and resulting surface of ceramics in high humidity are very similar to those observed under liquid water lubrication [218]. For Al_2O_3 and ZrO_2, the wear rate is higher when lubricated with liquid water compared with humid air [232,233]. It was assumed that the tribochemical product is soluble and easily removed in water and thus the substrate loses the protection when lubricated with liquid water. Beside the promotion of

Figure 13. Characteristic optical profilometry images at 40% RH and line profiles of various balls surface (upper) and soda-lime-silica glass substrates (lower) after 400 cycles of scratching at an applied load of 0.2 N under 20%, 40%, and 90% humidity conditions. (a) Si_3N_4 ball, (b) Al_2O_3 ball, and (c) 440C stainless steel ball [188].

9. Advanced Ceramics

High hardness and mechanical strength of advanced ceramics are traits that make them suitable for tribo-materials [200,201]. Among various types of advanced ceramics, the tribological properties of Al_2O_3, Si_3N_4, SiC and ZrO_2 are studied most extensively [200–212]. The wear mechanisms of these advanced ceramics can be categorized into three main types: (i) Mechanical fracture under high stress; (ii) wear debris induced third-body abrasion; and (iii) material removal due to tribochemical reactions [201]. The mild wear mainly takes place by fine wear debris and tribochemistry, while the severe wear happens with relative large size wear debris due to mechanical cracking and subsequent abrasion [200,201].

The investigation of effect of humidity on tribological properties of advanced ceramics mainly started in 1980s. Generally, when advanced ceramics are tested in unlubricated conditions, friction and wear decrease as environmental humidity increases [213–226]. It was found that the worn surface in low humidity conditions is rough, but it is relatively smoother in high humidity conditions due to tribochemical reactions involving the adsorbed water molecules. For Al_2O_3 surfaces, the main tribochemical reaction product is $Al(OH)_3$ [219,220,227]. For Si_3N_4 and SiC surfaces, the main products are SiO_2 and $Si(OH)_4$ [213–216,228–231]. It was believed that these hydroxide species are lubricious and could work as a protective or sacrificial layer to prevent the substrate from further wear. Therefore, the wear mechanism appears to gradually change from mechanical to tribochemical as environmental humidity increases. It may also explain why the degradation behavior and resulting surface of ceramics in high humidity are very similar to those observed under liquid water lubrication [218]. For Al_2O_3 and ZrO_2, the wear rate is higher when lubricated with liquid water compared with humid air [232,233]. It was assumed that the tribochemical product is soluble and easily removed in water and thus the

tribochemical reactions on the ceramics surface, it was also reported that a humid environment can promote adhesion between the fine debris particles [222], which may further strengthen the lubrication ability of the tribolayer.

10. Metals

The tribological applications of metals or alloys are usually associated with oil lubrications [234–240]; thus, studies on the effect of humidity on friction and wear behaviors of metallic substrates are conducted less extensively. Most research focuses on steel interfaces. In general, friction and wear of steel surfaces decrease with increasing humidity [241–244]. Klaffe investigated the wear behavior of AISI 52100 steel using a ball-on-flat tribometer over a wide RH range (3~100%) [242]. Although COF did not show a strong humidity dependence, wear increased drastically when humidity was below 15%. Further reducing humidity from 15% to 3% led to an increase in wear by factor of 4 [242]. The humidity effect on wear of various carbon steels also shows a similar trend—a severe wear at low humidity and a mild wear at high humidity [245]. In the intermediate region (45~65% RH), the friction coefficient appears to decrease marginally. It was suggested that water can facilitate the oxide layer formation on the steel worn surface and reduce adhesive wear and friction force [246,247]. In contrast, the nascent surfaces usually present severe adhesion behavior, which gives rise to high friction force [248].

11. Perspectives

Reviewing the literature reporting friction and wear behaviors of various types of materials in humid environments clearly reveals that the tribological behaviors cannot be explained or predicted with the mechanical properties of the materials being sheared at the sliding interface. The water molecules adsorbed at the surface and being sheared at the tribological interface paly pivotal roles, determining the magnitude of friction force and wear volume. For graphite, graphene, and UNCD, water can passivate the active dangling bonds when such defect sites are produced during the shear. Thus, it can mitigate wear problems, and lead to lower friction and wear. In the case of DLC, the effect of water depends on the hydrogen content in DLC (or in the test environment) and the counter surface. For TMDs, water appears to adsorb (or selectively react) at the edge sites and enhance the adhesion between adjacent layers and raise friction and wear. In the case of boron-based materials (h-BN, B_2O_3, and H_3BO_3), the adsorption and reaction of water molecules impinging from the gas phase govern the friction and wear behavior. The friction and wear behavior of silicon, silicon oxide, and silicate surfaces in humid air are even more complicated due to variations of possible reaction pathways depending on substrate chemistry, adsorbed water layer activity, and counter surface chemistry. For ceramics and metals, the tribochemical reaction products between water and the tribo-materials often work as a protective film, reducing friction and wear.

Considering the complexity of water activity (thickness and structure of physisorbed water as well as chemisorption and reaction of water at the interface under mechanical shear), it is not possible to explain the effects of water adsorption on various materials with one simple mechanism. The only obvious conclusion that can be made here is that its effect cannot be ignored and it is not sufficient to report that experiments were carried out in a humidity controlled condition. Details in molecular mechanisms of friction and wear behaviors of materials in humid air can be obtained only through carefully-designed and well-controlled experiments for specific questions, coupled with computational simulations with proper potential fields.

Funding: This work was supported by the National Science Foundation (Grant No. CMMI-1435766, 1727571 and DMR-1609107).

Acknowledgments: S.H.K. acknowledges the support from the One Thousand Talents Program of China.

Conflicts of Interest: The authors declare no conflict of interest.

References

1. Lancaster, J.K. A review of the influence of environmental humidity and water on friction, lubrication and wear. *Tribol. Int.* **1990**, *23*, 371–389. [CrossRef]
2. Bracken, E.F. Humidity control prevents ac brush disintegration. *Electr. World* **1933**, *102*, 410.
3. Dobson, J. The effect of humidity on brush operation. *Electr. J.* **1935**, *32*, 134.
4. Ramadanoff, D.; Glass, S.W. High-altitude brush problem. *Electr. Eng.* **1944**, *63*, 825–829. [CrossRef]
5. Savage, R.H. Graphite lubrication. *J. Appl. Phys.* **1948**, *19*, 1–10. [CrossRef]
6. Bowden, F.P.; Young, J.E. Friction of diamond, graphite, and carbon and the influence of surface films. *Proc. R. Soc. Lond. Ser. A* **1951**, *208*, 444–455. [CrossRef]
7. Savage, R.H.; Schaefer, D.L. Vapor lubrication of graphite sliding contacts. *J. Appl. Phys.* **1956**, *27*, 136–138. [CrossRef]
8. Deacon, R.F.; Goodman, J.F. Lubrication by lamellar solids. *Proc. R. Soc. Lond. Ser. A* **1958**, *243*, 464–482. [CrossRef]
9. Rowe, G. Some observations on the frictional behaviour of boron nitride and of graphite. *Wear* **1960**, *3*, 274–285. [CrossRef]
10. Bryant, P.; Gutshall, P.; Taylor, L. A study of mechanisms of graphite friction and wear. *Wear* **1964**, *7*, 118–126. [CrossRef]
11. Kumar, N.; Dash, S.; Tyagi, A.K.; Raj, B. Super low to high friction of turbostratic graphite under various atmospheric test conditions. *Tribol. Int.* **2011**, *44*, 1969–1978. [CrossRef]
12. Arnell, R.D.; Teer, D.G. Lattice parameters of graphite in relation to friction and wear. *Nature* **1968**, *218*, 1155–1156. [CrossRef]
13. Yen, B.K.; Schwickert, B.E.; Toney, M.F. Origin of low-friction behavior in graphite investigated by surface X-ray diffraction. *Appl. Phys. Lett.* **2004**, *84*, 4702–4704. [CrossRef]
14. Lancaster, J.K. Transitions in the friction and wear of carbons and graphites sliding against themselves. *ASLE Trans.* **1975**, *18*, 187–201. [CrossRef]
15. Lancaster, J. The wear of carbons and graphites. In *Treatise on Materials Science & Technology*; Scott, D., Ed.; Academic Press: New York, NY, USA, 1979; Volume 13, pp. 141–174.
16. Lancaster, J.K.; Pritchard, J.R. On the dusting wear regime of graphite sliding against carbon. *J. Phys. D Appl. Phys.* **1980**, *13*, 1551–1564. [CrossRef]
17. Lancaster, J.K.; Pritchard, J.R. The influence of environment and pressure on the transition to dusting wear of graphite. *J. Phys. D Appl. Phys.* **1981**, *14*, 747–762. [CrossRef]
18. Lepage, J.; Zaïdi, H. Influence of water vapour adsorption on the boundary conditions in tribology. In *Proceedings of the 14th Leeds-Lyon Symposium on Interface Dynamics*; Dowson, D., Taylor, C.M., Godet, M., Berthe, D., Eds.; Elsevier: Amsterdam, The Netherlands, 1988; pp. 259–266.
19. Allouche, A.; Ferro, Y. Dissociative adsorption of small molecules at vacancies on the graphite (0001) surface. *Carbon* **2006**, *44*, 3320–3327. [CrossRef]
20. Cabrera-Sanfelix, P.; Darling, G.R. Dissociative adsorption of water at vacancy defects in graphite. *J. Phys. Chem. C* **2007**, *111*, 18258–18263. [CrossRef]
21. Gurel, H.H.; Ozcelik, V.O.; Ciraci, S. Dissociative adsorption of molecules on graphene and silicene. *J. Phys. Chem. C* **2014**, *118*, 27574–27582. [CrossRef]
22. Levita, G.; Restuccia, P.; Righi, M.C. Graphene and MoS_2 interacting with water: A comparison by ab initio calculations. *Carbon* **2016**, *107*, 878–884. [CrossRef]
23. Rietsch, J.C.; Brender, P.; Dentzer, J.; Gadiou, R.; Vidal, L.; Vix-Guterl, C. Evidence of water chemisorption during graphite friction under moist conditions. *Carbon* **2013**, *55*, 90–97. [CrossRef]
24. Kim, K.S.; Lee, H.J.; Lee, C.; Lee, S.K.; Jang, H.; Ahn, J.H.; Kim, J.H.; Lee, H.J. Chemical vapor deposition-grown graphene: The thinnest solid lubricant. *ACS Nano* **2011**, *5*, 5107–5114. [CrossRef] [PubMed]
25. Berman, D.; Erdemir, A.; Sumant, A.V. Few layer graphene to reduce wear and friction on sliding steel surfaces. *Carbon* **2013**, *54*, 454–459. [CrossRef]
26. Bhowmick, S.; Banerji, A.; Alpas, A.T. Role of humidity in reducing sliding friction of multilayered graphene. *Carbon* **2015**, *87*, 374–384. [CrossRef]

27. Huang, Y.H.; Yao, Q.Z.; Qi, Y.Z.; Cheng, Y.; Wang, H.T.; Li, Q.Y.; Meng, Y.G. Wear evolution of monolayer graphene at the macroscale. *Carbon* **2017**, *115*, 600–607. [CrossRef]
28. Li, Z.Y.; Yang, W.J.; Wu, Y.P.; Wu, S.B.; Cai, Z.B. Role of humidity in reducing the friction of graphene layers on textured surfaces. *Appl. Surf. Sci.* **2017**, *403*, 362–370. [CrossRef]
29. Egberts, P.; Ye, Z.J.; Liu, X.Z.; Dong, Y.L.; Martini, A.; Carpick, R.W. Environmental dependence of atomic-scale friction at graphite surface steps. *Phys. Rev. B* **2013**, *88*, 035409. [CrossRef]
30. Liu, S.W.; Wang, H.P.; Xu, Q.; Ma, T.B.; Yu, G.; Zhang, C.; Geng, D.; Yu, Z.; Zhang, S.; Wang, W.; et al. Robust microscale superlubricity under high contact pressure enabled by graphene-coated microsphere. *Nat. Commun.* **2017**, *8*, 14029. [CrossRef] [PubMed]
31. Jacob, W.; Möller, W. On the structure of thin hydrocarbon films. *Appl. Phys. Lett.* **1993**, *63*, 1771–1773. [CrossRef]
32. Kumar, S.; Sarangi, D.; Dixit, P.N.; Panwar, O.S.; Bhattacharyya, R. Diamond-like carbon films with extremely low stress. *Thin Solid Films* **1999**, *346*, 130–137. [CrossRef]
33. Robertson, J. Diamond-like amorphous carbon. *Mater. Sci. Eng. R* **2002**, *37*, 129–281. [CrossRef]
34. Ban, M.; Hasegawa, T.; Fujii, S.; Fujioka, J. Stress and structural properties of diamond-like carbon films deposited by electron beam excited plasma CVD. *Diamond Relat. Mater.* **2003**, *12*, 47–56. [CrossRef]
35. Ferrari, A.C.; Robertson, J. Raman spectroscopy of amorphous, nanostructured, diamond-like carbon, and nanodiamond. *Philos. Trans. R. Soc. A* **2004**, *362*, 2477–2512. [CrossRef] [PubMed]
36. Oka, Y.; Kirinuki, M.; Nishimura, Y.; Azuma, K.; Fujiwara, E.; Yatsuzuka, M. Measurement of residual stress in DLC films prepared by plasma-based ion implantation and deposition. *Surf. Coat. Technol.* **2004**, *186*, 141–145. [CrossRef]
37. Ferrari, A.C. Non-destructive characterisation of carbon films. In *Tribology of Diamond-Like Carbon Films*; Donnet, C., Erdemir, A., Eds.; Springer: Boston, MA, USA, 2008; pp. 25–82.
38. Yang, M.; Marino, M.J.; Bojan, V.J.; Eryilmaz, O.L.; Erdemir, A.; Kim, S.H. Quantification of oxygenated species on a diamond-like carbon (DLC) surface. *Appl. Surf. Sci.* **2011**, *257*, 7633–7638. [CrossRef]
39. Ala'A, A.-A.; Eryilmaz, O.; Erdemir, A.; Kim, S.H. Nano-texture for a wear-resistant and near-frictionless diamond-like carbon. *Carbon* **2014**, *73*, 403–412.
40. Erdemir, A.; Switala, M.; Wei, R.; Wilbur, P. A tribological investigation of the graphite-to-diamond-like behavior of amorphous-carbon films ion-beam deposited on ceramic substrates. *Surf. Coat. Technol.* **1991**, *50*, 17–23. [CrossRef]
41. Donnet, C.; Belin, M.; Auge, J.C.; Martin, J.M.; Grill, A.; Patel, V. Tribochemistry of diamond-like carbon coatings in various environments. *Surf. Coat. Technol.* **1994**, *68*, 626–631. [CrossRef]
42. Ronkainen, H.; Koskinen, J.; Likonen, J.; Varjus, S.; Vihersalo, J. Characterization of wear surfaces in dry sliding of steel and alumina on hydrogenated and hydrogen-free carbon-films. *Diamond Relat. Mater.* **1994**, *3*, 1329–1336. [CrossRef]
43. Harris, S.J.; Weiner, A.M.; Meng, W.J. Tribology of metal-containing diamond-like carbon coatings. *Wear* **1997**, *211*, 208–217. [CrossRef]
44. Voevodin, A.A.; Donley, M.S.; Zabinski, J.S. Pulsed laser deposition of diamond-like carbon wear protective coatings: A review. *Surf. Coat. Technol.* **1997**, *92*, 42–49. [CrossRef]
45. Donnet, C.; Le Mogne, T.; Ponsonnet, L.; Belin, M.; Grill, A.; Patel, V.; Jahnes, C. The respective role of oxygen and water vapor on the tribology of hydrogenated diamond-like carbon coatings. *Tribol. Lett.* **1998**, *4*, 259–265. [CrossRef]
46. Venkatraman, C.; Brodbeck, C.; Lei, R. Tribological properties of diamond-like nanocomposite coatings at high temperatures. *Surf. Coat. Technol.* **1999**, *115*, 215–221. [CrossRef]
47. Kim, H.I.; Lince, J.R.; Eryilmaz, O.L.; Erdemir, A. Environmental effects on the friction of hydrogenated DLC films. *Tribol. Lett.* **2006**, *21*, 51–56. [CrossRef]
48. Eryilmaz, O.L.; Erdemir, A. Surface analytical investigation of nearly-frictionless carbon films after tests in dry and humid nitrogen. *Surf. Coat. Technol.* **2007**, *201*, 7401–7407. [CrossRef]
49. Erdemir, A. The role of hydrogen in tribological properties of diamond-like carbon films. *Surf. Coat. Technol.* **2001**, *146*, 292–297. [CrossRef]
50. Erdemir, A. Genesis of superlow friction and wear in diamondlike carbon films. *Tribol. Int.* **2004**, *37*, 1005–1012. [CrossRef]

51. Andersson, J.; Erck, R.A.; Erdemir, A. Friction of diamond-like carbon films in different atmospheres. *Wear* **2003**, *254*, 1070–1075. [CrossRef]
52. Andersson, J.; Erck, R.A.; Erdemir, A. Frictional behavior of diamondlike carbon films in vacuum and under varying water vapor pressure. *Surf. Coat. Technol.* **2003**, *163*, 535–540. [CrossRef]
53. Enke, K.; Dimigen, H.; Hubsch, H. Frictional properties of diamondlike carbon layers. *Appl. Phys. Lett.* **1980**, *36*, 291–292. [CrossRef]
54. Le Huu, T.; Zaidi, H.; Paulmier, D.; Voumard, P. Transformation of sp^3 to sp^2 sites of diamond like carbon coatings during friction in vacuum and under water vapour environment. *Thin Solid Films* **1996**, *290*, 126–130. [CrossRef]
55. Ronkainen, H.; Varjus, S.; Holmberg, K. Friction and wear properties in dry, water- and oil-lubricated DLC against alumina and DLC against steel contacts. *Wear* **1998**, *222*, 120–128. [CrossRef]
56. Zhang, W.; Tanaka, A.; Wazumi, K.; Koga, Y. Tribological properties of diamond-like carbon films in low and high moist air. *Tribol. Lett.* **2003**, *14*, 123–130. [CrossRef]
57. Li, H.; Xu, T.; Wang, C.; Chen, J.; Zhou, H.; Liu, H. Tribochemical effects on the friction and wear behaviors of diamond-like carbon film under high relative humidity condition. *Tribol. Lett.* **2005**, *19*, 231–238. [CrossRef]
58. Li, H.; Xu, T.; Wang, C.; Chen, J.; Zhou, H.; Liu, H. Friction-induced physical and chemical interactions among diamond-like carbon film, steel ball and water and/or oxygen molecules. *Diamond Relat. Mater.* **2006**, *15*, 1228–1234. [CrossRef]
59. Uchidate, M.; Liu, H.; Iwabuchi, A.; Yamamoto, K. Effects of water environment on tribological properties of DLC rubbed against stainless steel. *Wear* **2007**, *263*, 1335–1340. [CrossRef]
60. Wu, X.; Ohana, T.; Tanaka, A.; Kubo, T.; Nanao, H.; Minami, I.; Mori, S. Tribochemical investigation of DLC coating in water using stable isotopic tracers. *Appl. Surf. Sci.* **2008**, *254*, 3397–3402. [CrossRef]
61. Scharf, T.W.; Singer, I.L. Role of the transfer film on the friction and wear of metal carbide reinforced amorphous carbon coatings during run-in. *Tribol. Lett.* **2009**, *36*, 43–53. [CrossRef]
62. Cui, L.C.; Lu, Z.B.; Wang, L.P. Environmental effect on the load-dependent friction behavior of a diamond-like carbon film. *Tribol. Int.* **2015**, *82*, 195–199. [CrossRef]
63. Alazizi, A.; Draskovics, A.; Ramirez, G.; Erdemir, A.; Kim, S.H. Tribochemistry of carbon films in oxygen and humid environments: Oxidative wear and galvanic corrosion. *Langmuir* **2016**, *32*, 1996–2004. [CrossRef] [PubMed]
64. Kim, D.; Fischer, T.; Gallois, B. The effects of oxygen and humidity on friction and wear of diamond-like carbon films. In *Metallurgical Coatings and Thin Films*; McGuire, G.E., McIntyre, D.C., Hofmann, S., Eds.; Elsevier: Amsterdam, The Netherlands, 1991; pp. 537–542.
65. Liu, E.; Ding, Y.F.; Li, L.; Blanpain, B.; Celis, J.P. Influence of humidity on the friction of diamond and diamond-like carbon materials. *Tribol. Int.* **2007**, *40*, 216–219. [CrossRef]
66. Wang, X.; Wang, P.; Zhang, B.; Yang, S.R.; Zhang, J.Y. The tribological properties of fullerene-like hydrogenated carbon (FL-C:H) film under different humidity conditions. *Tribol. Trans.* **2009**, *52*, 354–359. [CrossRef]
67. Yi, J.; Kim, J.K.; Moon, M.W.; Lee, K.R.; Kim, S.S. Tribological performance of alternating-layered Si-DLC/DLC films under humid conditions. *Tribol. Lett.* **2009**, *34*, 223–228. [CrossRef]
68. Park, S.J.; Lee, K.R.; Ko, D.H. Tribochemical reaction of hydrogenated diamond-like carbon films: A clue to understand the environmental dependence. *Tribol. Int.* **2004**, *37*, 913–921. [CrossRef]
69. Erdemir, A.; Eryilmaz, O.L.; Nilufer, I.B.; Fenske, G.R. Synthesis of superlow-friction carbon films from highly hydrogenated methane plasmas. *Surf. Coat. Technol.* **2000**, *133*, 448–454. [CrossRef]
70. Gilmore, R.; Hauert, R. Control of the tribological moisture sensitivity of diamond-like carbon films by alloying with F, Ti or Si. *Thin Solid Films* **2001**, *398*, 199–204. [CrossRef]
71. Yang, S.H.; Kong, H.; Lee, K.R.; Park, S.; Kim, D.E. Effect of environment on the tribological behavior of Si-incorporated diamond-like carbon films. *Wear* **2002**, *252*, 70–79. [CrossRef]
72. Voevodin, A.A.; Phelps, A.W.; Zabinski, J.S.; Donley, M.S. Friction induced phase transformation of pulsed laser deposited diamond-like carbon. *Diamond Relat. Mater.* **1996**, *5*, 1264–1269. [CrossRef]
73. Koskinen, J.; Ronkainen, H.; Varjus, S.; Muukkonen, T.; Holmberg, K.; Sajavaara, T. Low friction ta-C films with hydrogen reservoirs. *Diamond Relat. Mater.* **2001**, *10*, 1030–1035. [CrossRef]
74. Gharam, A.A.; Lukitsch, M.; Qi, Y.; Alpas, A. Role of oxygen and humidity on the tribo-chemical behaviour of non-hydrogenated diamond-like carbon coatings. *Wear* **2011**, *271*, 2157–2163. [CrossRef]

75. Gardos, M.N.; Gabelich, S.A. Atmospheric effects of friction, friction noise and wear with silicon and diamond. Part III. SEM tribometry of polycrystalline diamond in vacuum and hydrogen. *Tribol. Lett.* **1999**, *6*, 103–112. [CrossRef]
76. Sumant, A.V.; Krauss, A.R.; Gruen, D.M.; Auciello, O.; Erdemir, A.; Williams, M.; Artiles, A.F.; Adams, W. Ultrananocrystalline diamond film as a wear-resistant and protective coating for mechanical seal applications. *Tribol. Trans.* **2005**, *48*, 24–31. [CrossRef]
77. Kumar, N.; Panda, K.; Dash, S.; Popov, C.; Reithmaier, J.P.; Panigrahi, B.K.; Tyagi, A.K.; Raj, B. Tribological properties of nanocrystalline diamond films deposited by hot filament chemical vapor deposition. *AIP Adv.* **2012**, *2*, 032164. [CrossRef]
78. Konicek, A.R.; Grierson, D.S.; Sumant, A.V.; Friedmann, T.A.; Sullivan, J.P.; Gilbert, P.U.P.A.; Sawyer, W.G.; Carpick, R.W. Influence of surface passivation on the friction and wear behavior of ultrananocrystalline diamond and tetrahedral amorphous carbon thin films. *Phys. Rev. B* **2012**, *85*, 155448. [CrossRef]
79. Radhika, R.; Kumar, N.; Sankaran, K.J.; Dumpala, R.; Dash, S.; Rao, M.S.R.; Arivuoli, D.; Tyagi, A.K.; Tai, N.H.; Lin, I.N. Extremely high wear resistance and ultra-low friction behaviour of oxygen-plasma-treated nanocrystalline diamond films. *J. Phys. D Appl. Phys.* **2013**, *46*, 425304. [CrossRef]
80. Rani, R.; Kumar, N.; Kozakov, A.T.; Googlev, K.A.; Sankaran, K.J.; Das, P.K.; Dash, S.; Tyagi, A.K.; Lin, I.N. Superlubrication properties of ultra-nanocrystalline diamond film sliding against a zirconia ball. *RSC Adv.* **2015**, *5*, 100663–100673. [CrossRef]
81. Gardos, M.N.; Soriano, B.L. The effect of environment on the tribological properties of polycrystalline diamond films. *J. Mater. Res.* **1990**, *5*, 2599–2609. [CrossRef]
82. Erdemir, A.; Fenske, G.R.; Krauss, A.R.; Gruen, D.M.; McCauley, T.; Csencsits, R.T. Tribological properties of nanocrystalline diamond films. *Surf. Coat. Technol.* **1999**, *120*, 565–572. [CrossRef]
83. Grillo, S.E.; Field, J.E. The friction of cvd diamond at high hertzian stresses: The effect of load, environment and sliding velocity. *J. Phys. D Appl. Phys.* **2000**, *33*, 595–602. [CrossRef]
84. Chromik, R.R.; Winfrey, A.L.; Luning, J.; Nemanich, R.J.; Wahl, K.J. Run-in behavior of nanocrystalline diamond coatings studied by in situ tribometry. *Wear* **2008**, *265*, 477–489. [CrossRef]
85. Konicek, A.R.; Grierson, D.S.; Gilbert, P.U.; Sawyer, W.G.; Sumant, A.V.; Carpick, R.W. Origin of ultralow friction and wear in ultrananocrystalline diamond. *Phys. Rev. Lett.* **2008**, *100*, 235502. [CrossRef] [PubMed]
86. Qi, Y.; Konca, E.; Alpas, A.T. Atmospheric effects on the adhesion and friction between non-hydrogenated diamond-like carbon (DLC) coating and aluminum—A first principles investigation. *Surf. Sci.* **2006**, *600*, 2955–2965. [CrossRef]
87. De Barros Bouchet, M.-I.; Zilibotti, G.; Matta, C.; Righi, M.C.; Vandenbulcke, L.; Vacher, B.; Martin, J.-M. Friction of diamond in the presence of water vapor and hydrogen gas. Coupling gas-phase lubrication and first-principles studies. *J. Phys. Chem. C* **2012**, *116*, 6966–6972. [CrossRef]
88. Salomon, G.; De Gee, A.W.J.; Zaat, J.H. Mechano-chemical factors in MoS_2 film lubrication. *Wear* **1964**, *7*, 87–101. [CrossRef]
89. Stewart, T.B.; Fleischauer, P.D. Chemistry of sputtered molybdenum-disulfide films. *Inorg. Chem.* **1982**, *21*, 2426–2431. [CrossRef]
90. Fleischauer, P.D. Effects of crystallite orientation on environmental stability and lubrication properties of sputtered MoS_2 thin-films. *ASLE Trans.* **1984**, *27*, 82–88. [CrossRef]
91. Peterson, M.B.; Johnson, R.L. *Friction and Wear Investigation of Molybdenum Disulfide II: Effects of Contaminants and Method of Application*; National Advisory Committee for Aeronautics: Washington, DC, USA, 1954.
92. Fusaro, R.L. Effect of substrate surface finish on the lubrication and failure mechanisms of molybdenum-disulfide films. *ASLE Trans.* **1982**, *25*, 141–156. [CrossRef]
93. Pardee, R.P. The effect of humidity on low-load frictional properties of a bonded solid film lubricant. *ASLE Trans.* **1972**, *15*, 130–142. [CrossRef]
94. Prasad, S.V.; McDevitt, N.T.; Zabinski, J.S. Tribology of tungsten disulfide films in humid environments: The role of a tailored metal-matrix composite substrate. *Wear* **1999**, *230*, 24–34. [CrossRef]
95. Haltner, A.J.; Oliver, C.S. Effect of water vapor on friction of molybdenum disulfide. *Ind. Eng. Chem. Fundam.* **1966**, *5*, 348–355. [CrossRef]
96. Roberts, E.W. Towards an optimised sputtered MoS_2 lubricant film. In *Proceedings of the 20th Aerospace Mechanics Symposium;* NASA, Lewis Research Center: Cleveland, OH, USA, 1986; pp. 103–119.

97. Uemura, M.; Saito, K.; Nakao, K. A mechanism of vapor effect on friction coefficient of molybdenum-disulfide. *Tribol. Trans.* **1990**, *33*, 551–556. [CrossRef]
98. Khare, H.S.; Burris, D.L. The effects of environmental water and oxygen on the temperature-dependent friction of sputtered molybdenum disulfide. *Tribol. Lett.* **2013**, *52*, 485–493. [CrossRef]
99. Khare, H.S.; Burris, D.L. Surface and subsurface contributions of oxidation and moisture to room temperature friction of molybdenum disulfide. *Tribol. Lett.* **2014**, *53*, 329–336. [CrossRef]
100. Luan, B.Q.; Zhou, R.H. Wettability and friction of water on a MoS_2 nanosheet. *Appl. Phys. Lett.* **2016**, *108*, 131601. [CrossRef]
101. Ataca, C.; Ciraci, S. Dissociation of H_2O at the vacancies of single-layer MoS_2. *Phys. Rev. B* **2012**, *85*, 195410. [CrossRef]
102. Ghuman, K.K.; Yadav, S.; Singh, C.V. Adsorption and dissociation of H_2O on monolayered MoS_2 edges: Energetics and mechanism from ab initio simulations. *J. Phys. Chem. C* **2015**, *119*, 6518–6529. [CrossRef]
103. Schumacher, A.; Kruse, N.; Prins, R.; Meyer, E.; Luthi, R.; Howald, L.; Guntherodt, H.J.; Scandella, L. Influence of humidity on friction measurements of supported MoS_2 single layers. *J. Vac. Sci. Technol. B* **1996**, *14*, 1264–1267. [CrossRef]
104. Zhao, X.; Perry, S.S. The role of water in modifying friction within MoS_2 sliding interfaces. *ACS Appl. Mater. Interfaces* **2010**, *2*, 1444–1448. [CrossRef] [PubMed]
105. Feng, D.D.; Peng, J.F.; Liu, S.S.; Zheng, X.J.; Yan, X.Y.; He, W.Y. Influences of thickness, scanning velocity and relative humidity on the frictional properties of WS_2 nanosheets. *Mater. Res. Express* **2018**, *5*, 10. [CrossRef]
106. Fox, V.; Renevier, N.; Teer, D.; Hampshire, J.; Rigato, V. The structure of tribologically improved MoS_2–metal composite coatings and their industrial applications. *Surf. Coat. Technol.* **1999**, *116*, 492–497. [CrossRef]
107. Renevier, N.M.; Fox, V.C.; Teer, D.G.; Hampshire, J. Coating characteristics and tribological properties of sputter-deposited MoS_2/metal composite coatings deposited by closed field unbalanced magnetron sputter ion plating. *Surf. Coat. Technol.* **2000**, *127*, 24–37. [CrossRef]
108. Renevier, N.M.; Fox, V.C.; Teer, D.G.; Hampshire, J. Performance of low friction MoS_2/titanium composite coatings used in forming applications. *Mater. Des.* **2000**, *21*, 337–343. [CrossRef]
109. Simmonds, M.C.; Savan, A.; Pfluger, E.; Van Swygenhoven, H. Mechanical and tribological performance of MoS_2 co-sputtered composites. *Surf. Coat. Technol.* **2000**, *126*, 15–24. [CrossRef]
110. Renevier, N.M.; Hamphire, J.; Fox, V.C.; Witts, J.; Allen, T.; Teer, D.G. Advantages of using self-lubricating, hard, wear-resistant MoS_2-based coatings. *Surf. Coat. Technol.* **2001**, *142*, 67–77. [CrossRef]
111. Teer, D.G. New solid lubricant coatings. *Wear* **2001**, *251*, 1068–1074. [CrossRef]
112. Xu, S.S.; Gao, X.M.; Sun, J.Y.; Hu, M.; Wang, D.S.; Jiang, D.; Zhou, F.; Weng, L.J.; Liu, W.M. Comparative study of moisture corrosion to WS_2 and WS_2/Cu multilayer films. *Surf. Coat. Technol.* **2014**, *247*, 30–38. [CrossRef]
113. Singh, H.; Mutyala, K.C.; Mohseni, H.; Scharf, T.W.; Evans, R.D.; Doll, G.L. Tribological performance and coating characteristics of sputter-deposited Ti-doped MoS_2 in rolling and sliding contact. *Tribol. Trans.* **2015**, *58*, 767–777. [CrossRef]
114. Li, H.; Zhang, G.A.; Wang, L.P. Low humidity-sensitivity of MoS_2/Pb nanocomposite coatings. *Wear* **2016**, *350–351*, 1–9. [CrossRef]
115. Ren, S.M.; Li, H.; Cui, M.J.; Wang, L.P.; Pu, J.B. Functional regulation of Pb-Ti/MoS_2 composite coatings for environmentally adaptive solid lubrication. *Appl. Surf. Sci.* **2017**, *401*, 362–372. [CrossRef]
116. Ding, X.Z.; Zeng, X.T.; He, X.Y.; Chen, Z. Tribological properties of Cr- and Ti-doped MoS_2 composite coatings under different humidity atmosphere. *Surf. Coat. Technol.* **2010**, *205*, 224–231. [CrossRef]
117. Ye, M.; Zhang, G.J.; Ba, Y.W.; Wang, T.; Wang, X.; Liu, Z.N. Microstructure and tribological properties of MoS_2+Zr composite coatings in high humidity environment. *Appl. Surf. Sci.* **2016**, *367*, 140–146. [CrossRef]
118. Niederhauser, P.; Hintermann, H.E.; Maillat, M. Moisture-resistant MoS_2-based composite lubricant films. *Thin Solid Films* **1983**, *108*, 209–218. [CrossRef]
119. Oñate, J.; Brizuela, M.; García-Luis, A.; Braceras, I.; Viviente, J.; Gomez-Elvira, J. Improved tribological behaviour of MoS_2 thin solid films alloyed with WC. In *Proceedings of the 9th European Space Mechanisms and Tribology Symposium*; ESA Publications Division: Noordwijk, The Netherlands, 2001; pp. 257–262.
120. Vierneusel, B.; Schneider, T.; Tremmel, S.; Wartzack, S.; Gradt, T. Humidity resistant MoS_2 coatings deposited by unbalanced magnetron sputtering. *Surf. Coat. Technol.* **2013**, *235*, 97–107. [CrossRef]

121. Domínguez-Meister, S.; Conte, M.; Igartua, A.; Rojas, T.; Sánchez-López, J. Self-lubricity of WSe_x nanocomposite coatings. *ACS Appl. Mater. Interfaces* **2015**, *7*, 7979–7986. [CrossRef] [PubMed]
122. Curry, J.F.; Argibay, N.; Babuska, T.; Nation, B.; Martini, A.; Strandwitz, N.C.; Dugger, M.T.; Krick, B.A. Highly oriented MoS_2 coatings: Tribology and environmental stability. *Tribol. Lett.* **2016**, *64*, 11. [CrossRef]
123. Kubart, T.; Polcar, T.; Kopecký, L.; Novák, R.; Nováková, D. Temperature dependence of tribological properties of and $MoSe_2$ coatings. *Surf. Coat. Technol.* **2005**, *193*, 230–233. [CrossRef]
124. Dominguez-Meister, S.; Rojas, T.C.; Brizuela, M.; Sanchez-Lopez, J.C. Solid lubricant behavior of MoS_2 and WSe_2-based nanocomposite coatings. *Sci. Technol. Adv. Mater.* **2017**, *18*, 122–133. [CrossRef] [PubMed]
125. Martin, J.M.; Lemogne, T.; Chassagnette, C.; Gardos, M.N. Friction of hexagonal boron-nitride in various environments. *Tribol. Trans.* **1992**, *35*, 462–472. [CrossRef]
126. Li, H.; Zeng, X.C. Wetting and interfacial properties of water nanodroplets in contact with graphene and monolayer boron-nitride sheets. *ACS Nano* **2012**, *6*, 2401–2409. [CrossRef] [PubMed]
127. Erdemir, A.; Fenske, G.; Erck, R. A study of the formation and self-lubrication mechanisms of boric acid films on boric oxide coatings. In *Metallurgical Coatings and Thin Films, Proceedings of the 17th International Conference on Metallurgical Coatings and 8th International Conference on Thin Films, San Diego, CA, USA*; Sartwell, B.D., Zemel, J.N., McGuire, G.E., Bresnock, F.N., Eds.; Elsevier: Amsterdam, The Netherlands, 1990; pp. 588–596.
128. Bindal, C.; Erdemir, A. Ultralow friction behavior of borided steel surfaces after flash annealing. *Appl. Phys. Lett.* **1996**, *68*, 923–925. [CrossRef]
129. Erdemir, A.; Bindal, C.; Fenske, G.R. Formation of ultralow friction surface films on boron carbide. *Appl. Phys. Lett.* **1996**, *68*, 1637–1639. [CrossRef]
130. Erdemir, A.; Halter, M.; Fenske, G.R. Preparation of ultralow-friction surface films on vanadium diboride. *Wear* **1997**, *205*, 236–239. [CrossRef]
131. Burroughs, B.R.; Kim, J.H.; Blanchet, T.A. Boric acid self-lubrication of B_2O_3-filled polymer composites. *Tribol. Trans.* **1999**, *42*, 592–600. [CrossRef]
132. Erdemir, A.; Eryilmaz, O.; Fenske, G. Self-replenishing solid lubricant films on boron carbide. *Surface Eng.* **1999**, *15*, 291–295. [CrossRef]
133. Huang, C.B.; Zhang, B.C.; Lan, H.; Du, L.Z.; Zhang, W.G. Friction properties of high temperature boride coating under dry air and water vapor ambiences. *Ceram. Int.* **2014**, *40*, 12403–12411. [CrossRef]
134. Ma, X.; Unertl, W.; Erdemir, A. The boron oxide–boric acid system: Nanoscale mechanical and wear properties. *J. Mater. Res.* **1999**, *14*, 3455–3466. [CrossRef]
135. Barthel, A.J.; Luo, J.W.; Kim, S.H. Origin of ultra-low friction of boric acid: Role of vapor adsorption. *Tribol. Lett.* **2015**, *58*. [CrossRef]
136. Bhushan, B. Nanotribology and nanomechanics of MEMS/NEMS and BioMEMS/BioNEMS materials and devices. *Microelectron. Eng.* **2007**, *84*, 387–412. [CrossRef]
137. Tanaka, M. An industrial and applied review of new MEMS devices features. *Microelectron. Eng.* **2007**, *84*, 1341–1344. [CrossRef]
138. Dong, P.; Chen, Y.-K.; Duan, G.-H.; Neilson, D.T. Silicon photonic devices and integrated circuits. *Nanophotonics* **2014**, *3*, 215–228. [CrossRef]
139. Bhushan, B. Nanotribology and nanomechanics. *Wear* **2005**, *259*, 1507–1531. [CrossRef]
140. Kim, S.H.; Asay, D.B.; Dugger, M.T. Nanotribology and MEMS. *Nano Today* **2007**, *2*, 22–29. [CrossRef]
141. Asay, D.B.; Dugger, M.T.; Kim, S.H. In-situ vapor-phase lubrication of MEMS. *Tribol. Lett.* **2008**, *29*, 67–74. [CrossRef]
142. Achanta, S.; Celis, J.-P. Nanotribology of MEMS/NEMS. In *Fundamentals of Friction and Wear on the Nanoscale*; Gnecco, E., Meyer, E., Eds.; Springer: New York, NY, USA, 2015; pp. 631–656.
143. Wang, X.; Yu, J.; Chen, L.; Qian, L.; Zhou, Z. Effects of water and oxygen on the tribochemical wear of monocrystalline Si(100) against SiO_2 sphere by simulating the contact conditions in MEMS. *Wear* **2011**, *271*, 1681–1688. [CrossRef]
144. Jin, C.; Yu, B.; Xiao, C.; Chen, L.; Qian, L. Temperature-dependent nanofabrication on silicon by friction-induced selective etching. *Nanoscale Res. Lett.* **2016**, *11*, 229. [CrossRef] [PubMed]
145. Chen, L.; He, X.; Liu, H.S.; Qian, L.M.; Kim, S.H. Water adsorption on hydrophilic and hydrophobic surfaces of silicon. *J. Phys. Chem. C* **2018**, *122*, 11385–11391. [CrossRef]
146. Asay, D.B.; Kim, S.H. Evolution of the adsorbed water layer structure on silicon oxide at room temperature. *J. Phys. Chem. B* **2005**, *109*, 16760–16763. [CrossRef] [PubMed]

147. Barnette, A.L.; Asay, D.B.; Kim, D.; Guyer, B.D.; Lim, H.; Janik, M.J.; Kim, S.H. Experimental and density functional theory study of the tribochemical wear behavior of SiO_2 in humid and alcohol vapor environments. *Langmuir* **2009**, *25*, 13052–13061. [CrossRef] [PubMed]
148. Alazizi, A.; Barthel, A.J.; Surdyka, N.D.; Luo, J.; Kim, S.H. Vapors in the ambient—A complication in tribological studies or an engineering solution of tribological problems? *Friction* **2015**, *3*, 85–114. [CrossRef]
149. Gräf, D.; Grundner, M.; Schulz, R. Reaction of water with hydrofluoric acid treated silicon (111) and (100) surfaces. *J. Vac. Sci. Technol. A* **1989**, *7*, 808–813. [CrossRef]
150. Mizuhara, K.; Hsu, S. Tribochemical reaction of oxygen and water on silicon surfaces. In *Wear Particles: From the Cradle to the Grave*; Dowson, D., Dalmaz, G., Childs, T.H.C., Taylor, C.M., Godet, M., Eds.; Elsevier: Amsterdam, The Netherlands, 1992; Volume 21, pp. 323–328.
151. Katsuki, F.; Kamei, K.; Saguchi, A.; Takahashi, W.; Watanabe, J. AFM studies on the difference in wear behavior between Si and SiO_2 in KOH solution. *J. Electrochem. Soc.* **2000**, *147*, 2328–2331. [CrossRef]
152. Katsuki, F. Single asperity tribochemical wear of silicon by atomic force microscopy. *J. Mater. Res.* **2009**, *24*, 173–178. [CrossRef]
153. Wen, J.L.; Ma, T.B.; Zhang, W.W.; Psofogiannakis, G.; van Duin, A.C.T.; Chen, L.; Qian, L.M.; Hu, Y.Z.; Lu, X.C. Atomic insight into tribochemical wear mechanism of silicon at the Si/SiO_2 interface in aqueous environment: Molecular dynamics simulations using ReaxFF reactive force field. *Appl. Surf. Sci.* **2016**, *390*, 216–223. [CrossRef]
154. Yeon, J.; van Duin, A.C.; Kim, S.H. Effects of water on tribochemical wear of silicon oxide interface: Molecular dynamics (MD) study with reactive force field (ReaxFF). *Langmuir* **2016**, *32*, 1018–1026. [CrossRef] [PubMed]
155. Wang, M.; Duan, F.L. Atomic-level wear behavior of sliding between silica (010) surfaces. *Appl. Surf. Sci.* **2017**, *425*, 1168–1175. [CrossRef]
156. Nevshupa, R.; Scherge, M.; Ahmed, S.-U. Transitional microfriction behavior of silicon induced by spontaneous water adsorption. *Surf. Sci.* **2002**, *517*, 17–28. [CrossRef]
157. Stempflé, P.; Domatti, A.; Dang, H.A.; Takadoum, J. Mechanical and chemical wear components in environmental multi-asperity nanotribology. *Tribol. Int.* **2015**, *82*, 358–374. [CrossRef]
158. Yu, B.J.; Li, X.Y.; Dong, H.S.; Chen, Y.F.; Qian, L.M.; Zhou, Z.R. Towards a deeper understanding of the formation of friction-induced hillocks on monocrystalline silicon. *J. Phys. D Appl. Phys.* **2012**, *45*, 145301. [CrossRef]
159. Yu, B.J.; Li, X.Y.; Dong, H.S.; Qian, L.M. Mechanical performance of friction-induced protrusive nanostructures on monocrystalline silicon and quartz. *Micro Nano Lett.* **2012**, *7*, 1270–1273. [CrossRef]
160. Marchand, D.J.; Chen, L.; Meng, Y.; Qian, L.; Kim, S.H. Effects of vapor environment and counter-surface chemistry on tribochemical wear of silicon wafers. *Tribol. Lett.* **2014**, *53*, 365–372. [CrossRef]
161. Chen, C.; Xiao, C.; Wang, X.D.; Zhang, P.; Chen, L.; Qi, Y.Q.; Qian, L.M. Role of water in the tribochemical removal of bare silicon. *Appl. Surf. Sci.* **2016**, *390*, 696–702. [CrossRef]
162. Xiao, C.; Guo, J.; Zhang, P.; Chen, C.; Chen, L.; Qian, L. Effect of crystal plane orientation on tribochemical removal of monocrystalline silicon. *Sci. Rep.* **2017**, *7*, 40750. [CrossRef] [PubMed]
163. Yu, J.; Kim, S.H.; Yu, B.; Qian, L.; Zhou, Z. Role of tribochemistry in nanowear of single-crystalline silicon. *ACS Appl. Mater. Interfaces* **2012**, *4*, 1585–1593. [CrossRef] [PubMed]
164. Xiao, C.; Chen, C.; Guo, J.; Zhang, P.; Chen, L.; Qian, L. Threshold contact pressure for the material removal on monocrystalline silicon by SiO_2 microsphere. *Wear* **2017**, *376–377*, 188–193. [CrossRef]
165. Chen, L.; Xiao, C.; Yu, B.; Kim, S.H.; Qian, L. What governs friction of silicon oxide in humid environment: Contact area between solids, water meniscus around the contact, or water layer structure? *Langmuir* **2017**, *33*, 9673–9679. [CrossRef] [PubMed]
166. Wang, X.; Kim, S.H.; Chen, C.; Chen, L.; He, H.; Qian, L. Humidity dependence of tribochemical wear of monocrystalline silicon. *ACS Appl. Mater. Interfaces* **2015**, *7*, 14785–14792. [CrossRef] [PubMed]
167. Chen, L.; Yang, Y.J.; He, H.T.; Kim, S.H.; Qian, L.M. Effect of coadsorption of water and alcohol vapor on the nanowear of silicon. *Wear* **2015**, *332*, 879–884. [CrossRef]
168. Chen, L.; He, H.; Wang, X.; Kim, S.H.; Qian, L. Tribology of Si/SiO_2 in humid air: Transition from severe chemical wear to wearless behavior at nanoscale. *Langmuir* **2014**, *31*, 149–156. [CrossRef] [PubMed]

169. Yu, J.X.; Chen, L.; Qian, L.M.; Song, D.L.; Cai, Y. Investigation of humidity-dependent nanotribology behaviors of Si(100)/SiO_2 pair moving from stick to slip. *Appl. Surf. Sci.* **2013**, *265*, 192–200. [CrossRef]
170. Wang, X.; Song, C.; Yu, B.; Chen, L.; Qian, L. Nanowear behaviour of monocrystalline silicon against SiO_2/Si tip in water. *Wear* **2013**, *298*, 80–86. [CrossRef]
171. Wang, X.D.; Guo, J.; Chen, C.; Chen, L.; Qian, L.M. A simple method to control nanotribology behaviors of monocrystalline silicon. *J. Appl. Phys.* **2016**, *119*, 044304. [CrossRef]
172. Baur, W.H. Variation of mean Si–O bond lengths in silicon–oxygen tetrahedra. *Acta Crystallogr. Sect. B Struct. Sci.* **1978**, *34*, 1751–1756. [CrossRef]
173. Asay, D.B.; Kim, S.H. Effects of adsorbed water layer structure on adhesion force of silicon oxide nanoasperity contact in humid ambient. *J. Chem. Phys.* **2006**, *124*, 174712. [CrossRef] [PubMed]
174. Dowson, D. *History of Tribology*; Addison-Wesley Longman Limited: London, UK, 1979.
175. Bowden, F.P.; Bowden, F.P.; Tabor, D. *The Friction and Lubrication of Solids*; Oxford University Press: Oxford, UK, 2001; Volume 1.
176. Barnette, A.L.; Asay, D.B.; Kim, S.H. Average molecular orientations in the adsorbed water layers on silicon oxide in ambient conditions. *Phys. Chem. Chem. Phys.* **2008**, *10*, 4981–4986. [CrossRef] [PubMed]
177. Chen, L.; Xiao, C.; He, X.; Yu, B.; Kim, S.H.; Qian, L. Friction and tribochemical wear behaviors of native oxide layer on silicon at nanoscale. *Tribol. Lett.* **2017**, *65*, 139. [CrossRef]
178. Chen, L.; Wen, J.; Zhang, P.; Yu, B.; Chen, C.; Ma, T.; Lu, X.; Kim, S.H.; Qian, L. Nanomanufacturing of silicon surface with a single atomic layer precision via mechanochemical reactions. *Nat. Commun.* **2018**, *9*, 1542. [CrossRef] [PubMed]
179. He, H.T.; Qian, L.M.; Pantano, C.G.; Kim, S.H. Mechanochemical wear of soda lime silica glass in humid environments. *J. Am. Ceram. Soc.* **2014**, *97*, 2061–2068. [CrossRef]
180. Shen, L.T.; Zhao, Y.D.; Wang, Y.; Song, R.B.; Yao, Q.; Chen, S.S.; Chai, Y. A long-term corrosion barrier with an insulating boron nitride monolayer. *J. Mater. Chem. A* **2016**, *4*, 5044–5050. [CrossRef]
181. Wiederhorn, S.M.; Bolz, L.H. Stress corrosion and static fatigue of glass. *J. Am. Ceram. Soc.* **1970**, *53*, 543–548. [CrossRef]
182. Michalske, T.A.; Freiman, S.W. A molecular mechanism for stress-corrosion in vitreous silica. *J. Am. Ceram. Soc.* **1983**, *66*, 284–288. [CrossRef]
183. Ciccotti, M. Stress-corrosion mechanisms in silicate glasses. *J. Phys. D Appl. Phys.* **2009**, *42*, 214006. [CrossRef]
184. Adams, R.; Mcmillan, P.W. Static fatigue in glass. *J. Mater. Sci.* **1977**, *12*, 643–657. [CrossRef]
185. Orowan, E. The fatigue of glass under stress. *Nature* **1944**, *154*, 341–343. [CrossRef]
186. Bradley, L.C.; Dilworth, Z.R.; Barnette, A.L.; Hsiao, E.; Barthel, A.J.; Pantano, C.G.; Kim, S.H. Hydronium ions in soda-lime silicate glass surfaces. *J. Am. Ceram. Soc.* **2013**, *96*, 458–463. [CrossRef]
187. Surdyka, N.D.; Pantano, C.G.; Kim, S.H. Environmental effects on initiation and propagation of surface defects on silicate glasses: Scratch and fracture toughness study. *Appl. Phys. A* **2014**, *116*, 519–528. [CrossRef]
188. He, H.T.; Qian, L.M.; Pantano, C.G.; Kim, S.H. Effects of humidity and counter-surface on tribochemical wear of soda-lime-silica glass. *Wear* **2015**, *342*, 100–106. [CrossRef]
189. Yu, J. Quantitative investigation on single-asperity friction and wear of phosphate lase glass against aspherical AFM diamond tip. *Tribol. Int.* **2015**, *81*, 43–52. [CrossRef]
190. He, H.; Luo, J.; Qian, L.; Pantano, C.G.; Kim, S.H. Thermal poling of soda-lime silica glass with nonblocking electrodes—Part 2: Effects on mechanical and mechanochemical properties. *J. Am. Ceram. Soc.* **2016**, *99*, 1231–1238. [CrossRef]
191. Yu, J.X.; He, H.T.; Jian, Q.Y.; Zhang, W.L.; Zhang, Y.F.; Yuan, W.F. Tribochemical wear of phosphate laser glass against silica ball in water. *Tribol. Int.* **2016**, *104*, 10–18. [CrossRef]
192. He, H.T.; Yu, J.X.; Qian, L.M.; Pantano, C.G.; Kim, S.H. Enhanced tribological properties of barium boroaluminosilicate glass by thermal poling. *Wear* **2017**, *376*, 337–342. [CrossRef]
193. Yu, J.X.; He, H.T.; Zhang, Y.F.; Hu, H.L. Nanoscale mechanochemical wear of phosphate laser glass against a CeO_2 particle in humid air. *Appl. Surf. Sci.* **2017**, *392*, 523–530. [CrossRef]
194. Luo, J.; He, H.; Podraza, N.J.; Qian, L.; Pantano, C.G.; Kim, S.H. Thermal poling of soda-lime silica glass with nonblocking electrodes—Part 1: Effects of sodium ion migration and water ingress on glass surface structure. *J. Am. Ceram. Soc.* **2016**, *99*, 1221–1230. [CrossRef]

195. Sheth, N.; Luo, J.W.; Banerjee, J.; Pantano, C.G.; Kim, S.H. Characterization of surface structures of dealkalized soda lime silica glass using X-ray photoelectron, specular reflection infrared, attenuated total reflection infrared and sum frequency generation spectroscopies. *J. Non-Cryst. Solids* **2017**, *474*, 24–31. [CrossRef]
196. Sheth, N.; Ngo, D.; Banerjee, J.; Zhou, Y.; Pantano, C.G.; Kim, S.H. Probing hydrogen-bonding interactions of water molecules adsorbed on silica, sodium calcium silicate, and calcium aluminosilicate glasses. *J. Phys. Chem. C* **2018**, in press. [CrossRef]
197. He, H.T.; Kim, S.H.; Qian, L.M. Effects of contact pressure, counter-surface and humidity on wear of soda-lime-silica glass at nanoscale. *Tribol. Int.* **2016**, *94*, 675–681. [CrossRef]
198. Archard, J.F. Contact and rubbing of flat surfaces. *J. Appl. Phys.* **1953**, *24*, 981–988. [CrossRef]
199. Archard, J.F.; Hirst, W. The wear of metals under unlubricated conditions. *Proc. R. Soc. Lond. Ser. A* **1956**, *236*, 397–410. [CrossRef]
200. Kato, K.; Adachi, K. Wear of advanced ceramics. *Wear* **2002**, *253*, 1097–1104. [CrossRef]
201. Fischer, T.E.; Zhu, Z.; Kim, H.; Shin, D.S. Genesis and role of wear debris in sliding wear of ceramics. *Wear* **2000**, *245*, 53–60. [CrossRef]
202. Buckley, D.H.; Miyoshi, K. Friction and wear of ceramics. *Wear* **1984**, *100*, 333–353. [CrossRef]
203. Fischer, T.E. Friction and wear of ceramics. *Scr. Metall. Mater.* **1990**, *24*, 833–838. [CrossRef]
204. Hsu, S.M.; Lim, D.S.; Wang, Y.S.; Munro, R.G. Ceramics wear maps—Concept and method development. *Lubr. Eng.* **1991**, *47*, 49–54.
205. Fischer, T.E.; Mullins, W.M. Chemical aspects of ceramic tribology. *J. Phys. Chem.* **1992**, *96*, 5690–5701. [CrossRef]
206. Lancaster, J.K.; Mashal, Y.A.H.; Atkins, A.G. The role of water in the wear of ceramics. *J. Phys. D Appl. Phys.* **1992**, *25*, A205–A211. [CrossRef]
207. Gogotsi, Y.G.; Yoshimura, M. Water effects on corrosion behavior of structural ceramics. *MRS Bull.* **1994**, *19*, 39–45. [CrossRef]
208. Klaffke, D. On the influence of test parameters on friction and wear of ceramics in oscillating sliding contacts. *Tribotest* **1995**, *1*, 311–320. [CrossRef]
209. Hsu, S.M.; Shen, M.C. Ceramic wear maps. *Wear* **1996**, *200*, 154–175. [CrossRef]
210. Adachi, K.; Kato, K.; Chen, N. Wear map of ceramics. *Wear* **1997**, *203*, 291–301. [CrossRef]
211. Erdemir, A.; Erck, R.; Fenske, G.; Hong, H. Solid/liquid lubrication of ceramics at elevated temperatures. *Wear* **1997**, *203*, 588–595. [CrossRef]
212. Xu, J.G.; Kato, K. Formation of tribochemical layer of ceramics sliding in water and its role for low friction. *Wear* **2000**, *245*, 61–75. [CrossRef]
213. Sugita, T.; Ueda, K.; Kanemura, Y. Material removal mechanism of silicon-nitride during rubbing in water. *Wear* **1984**, *97*, 1–8. [CrossRef]
214. Fischer, T.E.; Tomizawa, H. Interaction of tribochemistry and microfracture in the friction and wear of silicon-nitride. *Wear* **1985**, *105*, 29–45. [CrossRef]
215. Kapsa, P.; Enomoto, Y. Sliding damage on hot-pressed and sintered silicon-nitride caused by a diamond tip under controlled humidity. *Wear* **1988**, *127*, 65–83. [CrossRef]
216. Imada, Y.; Kamamura, K.; Honda, F.; Nakajima, K. The tribological reaction accompanying friction and wear of silicon-nitride containing titanium nitride. *J. Tribol.* **1992**, *114*, 230–235. [CrossRef]
217. Ishigaki, H.; Kawaguchi, I.; Iwasa, M.; Toibana, Y. Friction and wear of hot-pressed silicon-nitride and other ceramics. *J. Tribol.* **1986**, *108*, 514–521. [CrossRef]
218. Sasaki, S. The effects of the surrounding atmosphere on the friction and wear of alumina, zirconia, silicon-carbide and silicon-nitride. *Wear* **1989**, *134*, 185–200. [CrossRef]
219. Perez-Unzueta, A.; Beynon, J.; Gee, M. Effects of surrounding atmosphere on the wear of sintered alumina. *Wear* **1991**, *146*, 179–196. [CrossRef]
220. Gee, M.G. The formation of aluminium hydroxide in the sliding wear of alumina. *Wear* **1992**, *153*, 201–227. [CrossRef]
221. Park, D.S.; Danyluk, S.; Mcnallan, M.J. Influence of tribochemical reaction-products on friction and wear of silicon-nitride at elevated-temperatures in reactive environments. *J. Am. Ceram. Soc.* **1992**, *75*, 3033–3039. [CrossRef]
222. Komvopoulos, K.; Li, H. The effect of tribofilm formation and humidity on the friction and wear properties of ceramic materials. *J. Tribol.* **1992**, *114*, 131–140. [CrossRef]

223. Srinivasan, S.R.; Blau, P.J. Effect of relative-humidity on repetitive impact behavior of machined silicon-nitride. *J. Am. Ceram. Soc.* **1994**, *77*, 683–688. [CrossRef]
224. Basu, B.; Vitchev, R.G.; Vleugels, J.; Celis, J.P.; van der Biest, O. Influence of humidity on the fretting wear of self-mated tetragonal zirconia ceramics. *Acta Mater.* **2000**, *48*, 2461–2471. [CrossRef]
225. Murthy, V.S.R.; Kobayashi, H.; Tsurekawa, S.; Tamari, N.; Watanabe, T.; Kato, K. Influence of humidity and doping elements on the friction and wear of SiC in unlubricated sliding. *Tribol. Int.* **2004**, *37*, 353–364. [CrossRef]
226. Wäsche, R.; Klaffke, D.; Troczynski, T. Tribological performance of SiC and TiB_2 against SiC and Al_2O_3 at low sliding speeds. *Wear* **2004**, *256*, 695–704. [CrossRef]
227. Gates, R.S.; Hsu, S.M.; Klaus, E.E. Tribochemical mechanism of alumina with water. *Tribol. Trans.* **1989**, *32*, 357–363. [CrossRef]
228. Jahanmir, S.; Fischer, T.E. Friction and wear of silicon-nitride lubricated by humid air, water, hexadecane and hexadecane + 0.5 percent stearic acid. *Tribol. Trans.* **1988**, *31*, 32–43. [CrossRef]
229. Kimura, Y.; Okada, K.; Enomoto, Y. Sliding damage of silicon-nitride in plane contact. *Wear* **1989**, *133*, 147–161. [CrossRef]
230. Hah, S.R.; Fischer, T.E. Tribochemical polishing of silicon nitride. *J. Electrochem. Soc.* **1998**, *145*, 1708–1714. [CrossRef]
231. Fischer, T.E.; Liang, H.; Mullins, W.M. Tribochemical lubricious oxides on silicon nitride. *MRS Online Proc. Libr.* **2011**, *140*, 339–344. [CrossRef]
232. Wallbridge, N.; Dowson, D.; Roberts, E. The wear characteristics of sliding pairs of high density polycrystalline aluminium oxide under both dry and wet conditions. In Proceedings of the International Conference of Wear of Materials, Reston, VA, USA, 11–14 April 1983.
233. Fischer, T.E.; Anderson, M.P.; Jahanmir, S.; Salher, R. Friction and wear of tough and brittle zirconia in nitrogen, air, water, hexadecane and hexadecane containing stearic-acid. *Wear* **1988**, *124*, 133–148. [CrossRef]
234. Barnes, A.M.; Bartle, K.D.; Thibon, V.R. A review of zinc dialkyldithiophosphates (ZDDPs): Characterisation and role in the lubricating oil. *Tribol. Int.* **2001**, *34*, 389–395. [CrossRef]
235. Olver, A. Gear lubrication—A review. *Proc. Inst. Mech. Eng. Part J.* **2002**, *216*, 255–267. [CrossRef]
236. Spikes, H. The history and mechanisms of ZDDP. *Tribol. Lett.* **2004**, *17*, 469–489. [CrossRef]
237. Nicholls, M.A.; Do, T.; Norton, P.R.; Kasrai, M.; Bancroft, G.M. Review of the lubrication of metallic surfaces by zinc dialkyl-dithiophosphates. *Tribol. Int.* **2005**, *38*, 15–39. [CrossRef]
238. Chen, Z.; Liu, X.; Liu, Y.; Gunsel, S.; Luo, J. Ultrathin MoS_2 nanosheets with superior extreme pressure property as boundary lubricants. *Sci. Rep.* **2015**, *5*, 12869. [CrossRef] [PubMed]
239. Chen, Z.; Liu, Y.; Luo, J. Tribological properties of few-layer graphene oxide sheets as oil-based lubricant additives. *Chin. J. Mech. Eng.* **2016**, *29*, 439–444. [CrossRef]
240. Chen, Z.; Liu, Y.; Gunsel, S.; Luo, J. Mechanism of antiwear property under high pressure of synthetic oil-soluble ultrathin MoS_2 sheets as lubricant additives. *Langmuir* **2018**, *34*, 1635–1644. [CrossRef] [PubMed]
241. Goto, H.; Buckley, D.H. The influence of water-vapor in air on the friction behavior of pure metals during fretting. *Tribol. Int.* **1985**, *18*, 237–245. [CrossRef]
242. Klaffke, D. On the repeatability of friction and wear results and on the influence of humidity in oscillating sliding tests of steel steel pairings. *Wear* **1995**, *189*, 117–121. [CrossRef]
243. De Baets, P.; Kalacska, G.; Strijckmans, K.; van de Velde, F.; Van Peteghem, A.P. Experimental study by means of thin layer activation of the humidity influence on the fretting wear of steel surfaces. *Wear* **1998**, *216*, 131–137. [CrossRef]
244. Bregliozzi, G.; Di Schino, A.; Kenny, J.M.; Haefke, H. The influence of atmospheric humidity and grain size on the friction and wear of AISI 304 austenitic stainless steel. *Mater. Lett.* **2003**, *57*, 4505–4508. [CrossRef]
245. Oh, H.K.; Yeon, K.H.; Kim, H.Y. The influence of atmospheric humidity on the friction and wear of carbon steels. *J. Mater. Process. Technol.* **1999**, *95*, 10–16. [CrossRef]
246. Wang, Y.; Lei, T.Q. Wear behavior of steel 1080 with different microstructures during dry sliding. *Wear* **1996**, *194*, 44–53. [CrossRef]

247. Wang, Y.; Lei, T.Q.; Liu, J.J. Tribo-metallographic behavior of high carbon steels in dry sliding: I. Wear mechanisms and their transition. *Wear* **1999**, *231*, 1–11. [CrossRef]
248. Goto, H.; Amamoto, Y. Effect of varying load on wear resistance of carbon steel under unlubricated conditions. *Wear* **2003**, *254*, 1256–1266. [CrossRef]